Geochemistry Geophysics Geosystems G3
AN ELECTRONIC JOURNAL OF THE EARTH SCIENCES
Published by AGU and the Geochemical Society

Article
Volume 7, Number 11
3 November 2006
Q11N06, doi:10.1029/2005GC001228
ISSN: 1525-2027

A model-based interpretation of low-frequency changes in the carbon cycle during the last 120,000 years and its implications for the reconstruction of atmospheric $\Delta^{14}C$

Peter Köhler
Alfred Wegener Institute, Helmholtz Center for Polar and Marine Research, P.O. Box 120161, D-27515 Bremerhaven, Germany (pkoehler@awi-bremerhaven.de)

Raimund Muscheler
Climate and Global Dynamics Division—Paleoclimatology, National Center for Atmospheric Research, Boulder, Colorado, USA

Now at Climate and Radiation Branch, NASA Goddard Space Flight Center, Greenbelt, Maryland 20771, USA (raimund@climate.gsfc.nasa.gov)

Hubertus Fischer
Alfred Wegener Institute, Helmholtz Center for Polar and Marine Research, P.O. Box 120161, D-27515 Bremerhaven, Germany (hufischer@awi-bremerhaven.de)

[1] A main caveat in the interpretation of observed changes in atmospheric $\Delta^{14}C$ during the last 50,000 years is the unknown variability of the carbon cycle, which together with changes in the ^{14}C production rates determines the ^{14}C dynamics. A plausible scenario explaining glacial/interglacial dynamics seen in atmospheric CO_2 and $\delta^{13}C$ was proposed recently (Köhler et al., 2005a). A similar approach that expands its interpretation to the ^{14}C cycle is an important step toward a deeper understanding of $\Delta^{14}C$ variability. This approach is based on an ocean/atmosphere/biosphere box model of the global carbon cycle (BICYCLE) to reproduce low-frequency changes in atmospheric CO_2 as seen in Antarctic ice cores. The model is forced forward in time by various paleoclimatic records derived from ice and sediment cores. The simulation results of our proposed scenario match a compiled CO_2 record from various ice cores during the last 120,000 years with high accuracy ($r^2 = 0.89$). We analyze scenarios with different ^{14}C production rates, which are either constant or based on ^{10}Be measured in Greenland ice cores or the recent high-resolution geomagnetic field reconstruction GLOPIS-75 and compare them with the available $\Delta^{14}C$ data covering the last 50,000 years. Our results suggest that during the last glacial cycle in general less than 110‰ of the increased atmospheric $\Delta^{14}C$ is based on variations in the carbon cycle, while the largest part (5/6) of the variations has to be explained by other factors. Glacial atmospheric $\Delta^{14}C$ larger than 700‰ cannot not be explained within our framework, neither through carbon cycle-based changes nor through variable ^{14}C production. Superimposed on these general trends might lie positive anomalies in atmospheric $\Delta^{14}C$ of ~50‰ caused by millennial-scale variability of the northern deep water production during Heinrich events and Dansgaard/Oeschger climate fluctuations. According to our model, the dominant processes that increase glacial $\Delta^{14}C$ are a reduced glacial ocean circulation (+~40‰), a restricted glacial gas exchange between the atmosphere and the surface ocean through sea ice coverage (+~20‰), and the enrichment of dissolved inorganic carbon with ^{14}C in the surface waters through isotopic fractionation during higher glacial marine export production caused by iron fertilization (+~10‰).

Components: 14,593 words, 9 figures, 1 table.

Keywords: carbon cycle; ^{14}C cycle; ^{14}C production rates; glacial/interglacial; modeling; box model.

Index Terms: 0322 Atmospheric Composition and Structure: Constituent sources and sinks; 0428 Biogeosciences: Carbon cycling (4806); 0473 Biogeosciences: Paleoclimatology and paleoceanography (3344, 4900); 1615 Global Change: Biogeochemical cycles, processes, and modeling (0412, 0414, 0793, 4805, 4912); 4918 Paleoceanography: Cosmogenic isotopes (1150).

Received 20 December 2005; **Revised** 25 July 2006; **Accepted** 30 August 2006; **Published** 3 November 2006.

Köhler, P., R. Muscheler, and H. Fischer (2006), A model-based interpretation of low-frequency changes in the carbon cycle during the last 120,000 years and its implications for the reconstruction of atmospheric $\Delta^{14}C$, *Geochem. Geophys. Geosyst.*, *7*, Q11N06, doi:10.1029/2005GC001228.

Theme: Past Ocean Circulation
Guest Editors: Jean Lynch-Stieglitz, Catherine Kissel, and Olivier Marchal

1. Introduction

[2] New measurements from which the radiocarbon signal (^{14}C) of the atmosphere during the past thousands of years can be reconstructed were published steadily throughout the last years [*Bard et al.*, 1998; *Stuiver et al.*, 1998; *Voelker et al.*, 1998; *Goslar et al.*, 2000; *Hughen et al.*, 2000, 2004; *Kitagawa and van der Pflicht*, 2000; *Schramm et al.*, 2000; *Beck et al.*, 2001; *Reimer et al.*, 2004; *Fairbanks et al.*, 2005]. The reconstructions of past changes in the atmospheric ^{14}C concentration have a high accuracy for the Holocene period where the data are based on measurements of the $^{14}C/^{12}C$ ratios measured in dendrochronologically dated tree rings [*Reimer et al.*, 2004]. For the pre-Holocene period the various $\Delta^{14}C$ data sets (Figure 1) come from different natural archives. They exhibit increasing differences the further back in time they extend. The data for the last 10,000 years (10 kyr) show a moderate long-term decrease of the order of 100‰. Despite the differences between the $\Delta^{14}C$ reconstruction for the periods of the last glacial and deglaciation, a rather sharp increase of approximately 600‰ around 44 kyr BP to high values of the order of 400–800‰ from 40 to 20 kyr BP and a strong decrease from 20 to 10 kyr BP are consistent features of most of the records.

[3] The most important factor that can influence the atmospheric ^{14}C concentration is the variable ^{14}C production rate [*Siegenthaler et al.*, 1980] which is caused by changes in solar activity and the geomagnetic dipole field intensity provided that the galactic cosmic ray flux to the solar system stayed constant [*Lal and Peters*, 1967]. To our knowledge there are no clear indications for a variable galactic cosmic ray intensity during the last 50 kyr. Assuming that also the average solar modulation of the cosmic ray flux was constant, estimates of past changes in the ^{14}C production rate can be based on geomagnetic field records [*Laj et al.*, 2002]. Another approach is to use other radionuclide records from ice cores to estimate the ^{14}C production rate history [*Muscheler et al.*, 2004]. Especially ^{10}Be records from the polar ice caps have the potential to document solar and geomagnetic field changes [see, e.g., *Beer et al.*, 1990; *Wagner et al.*, 2000].

[4] Both approaches to estimate the ^{14}C production rate have advantages and disadvantages. As mentioned ^{10}Be records theoretically include all potential changes that also influence the ^{14}C production rate. However, climatic influences on these records could partly mask the production signal. In the cases of the Greenland Summit ^{10}Be records it is clear that the variable accumulation rate has a dominant influence on the ^{10}Be concentration [*Wagner et al.*, 2001]. At least during fast climate fluctuations in the northern hemisphere, the so-called Dansgaard/Oeschger events [*Johnsen et al.*, 1992], this obvious climatic influence can be at least removed partly by calculating the ^{10}Be flux [*Yiou et al.*, 1997; *Muscheler et al.*, 2000; *Wagner et al.*, 2001]. However, there still could be an influence of changes in atmospheric ^{10}Be transport or deposition on the ^{10}Be flux [*Field et al.*, 2006]. In addition, uncertainties in the accumulation rate estimates directly translate into uncertainties in the ^{10}Be flux.

[5] Geomagnetic field reconstructions could also contain uncorrected climatic influences as for

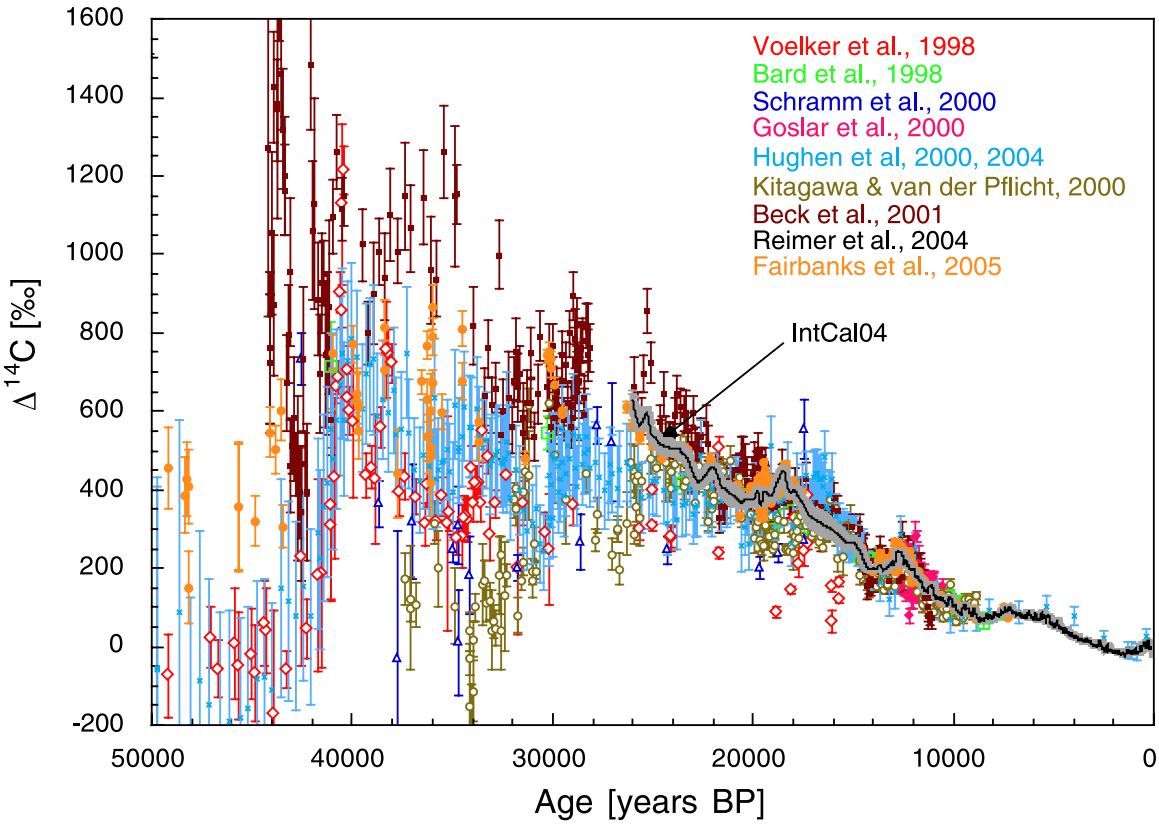

Figure 1. A compilation of published reconstructions of atmospheric $\Delta^{14}C$ during the last 50 kyr.

example due to a climatic influence on the acquisition of remanent magnetization by sediments [*Kok*, 1999]. In addition, since such records are also influenced by higher moments of the geomagnetic field, which are of minor importance for the ^{14}C production rate, several records are usually combined to remove or diminish local effects [*Laj et al.*, 2000; *Yang et al.*, 2000]. There are no continuous records for the last 60 kyr and different data sets have to be normalized and combined in order to use such a compiled record to estimate changes in the ^{14}C production rate. Differences between different records (e.g., in the chronology) lead to relatively large uncertainties also in the geomagnetic field-based reconstruction of the ^{14}C production rate [*Laj et al.*, 2002, 2005]. On longer timescales the ^{10}Be and geomagnetic field-based ^{14}C production rate reconstructions agree well. Nevertheless, there are differences that affect the interpretation of the causes for the $\Delta^{14}C$ changes due to the high sensitivity of $\Delta^{14}C$ to small production rate changes [*Muscheler et al.*, 2004].

[6] Another part of the climate system that changes atmospheric ^{14}C concentrations is the carbon cycle itself. Thus one caveat in the interpretation of atmospheric $\Delta^{14}C$ variations over the past thousands of years was always the lack of precise knowledge of changes in the carbon cycle. Some ^{14}C studies proposed significant changes in the global carbon cycle [e.g., *Beck et al.*, 2001; *Hughen et al.*, 2004; *Muscheler et al.*, 2004]. Especially changes in ocean circulation, gradually over time, or abrupt declines in northern deep water formation were proposed as hypotheses to explain either the long-term trend or millennial-scale variability in $\Delta^{14}C$. The positive anomaly in atmospheric $\Delta^{14}C$ during the Younger Dryas cold events (~12 kyr BP), for example, was suggested to be caused by a reduction of the Atlantic thermohaline circulation (THC) [e.g., *Marchal et al.*, 2001; *Delaygue et al.*, 2003]. However, most of these model-based scenarios were not challenged to reconstruct atmospheric CO_2 concentrations. As CO_2 was measured in Antarctic ice cores 650 kyr back in time [*Fischer et al.*, 1999; *Petit et al.*, 1999; *Indermühle et al.*, 1999, 2000; *Monnin et al.*, 2001; *Kawamura et al.*, 2003; *Siegenthaler et al.*, 2005] with an uncertainty of several ppmv only, it can be understood as

the ultimate paleo record. Therefore any interpretation of paleo records which assume massive climatic changes and as consequence impacts on the global carbon cycle should be discussed with respect of their implications for the temporal evolution of atmospheric CO_2.

[7] During the last four glacial cycles atmospheric CO_2 rose from its minima of 180 ppmv during glacial cold periods to its preindustrial maximum of 280–300 ppmv during interglacials [*Fischer et al.*, 1999; *Petit et al.*, 1999; *Monnin et al.*, 2001; *Kawamura et al.*, 2003]. The older CO_2 data measured recently in the EPICA Dome C ice core show similar glacial but lower interglacial values of about 250 to 260 ppmv connected to cooler interglacials during that time [*Siegenthaler et al.*, 2005]. The interpretation of this glacial/interglacial rise in CO_2 was challenging the scientific community throughout the last two decades. Various hypothesis were tested with models of different complexity to explain these observations (see reviews by *Archer et al.* [2000] and *Sigman and Boyle* [2000]), but a widely excepted interpretation remained elusive. The most recent approach [*Köhler et al.*, 2005a] applied a global carbon cycle box model for the first time in a transient mode and reproduced observed variations in atmospheric CO_2 and its carbon isotopes over the last glacial/interglacial transition from the LGM to the Holocene. In a second application forced with a different extended data set this approach was able to reproduce the low-frequency changes observed in CO_2 over the last 650 kyr (r^2 = 0.75) [*Köhler and Fischer*, 2006b; *Wolff et al.*, 2005]. Accordingly, this model study was able to identify important processes contributing to the glacial/interglacial change in CO_2 and proposed a scenario which might explain the observed changes in the carbon cycle. However, due to the simplicity of the model and the data uncertainties, alternative scenarios explaining atmospheric CO_2 for other reasons cannot be excluded. We therefore believe that carbon cycle dynamics over the last eight glacial cycles can nowadays be estimated by applying the same modeling approach. Thus one main caveat in the interpretation of atmospheric ^{14}C might be overcome and new conclusions can be drawn from a reinterpretation of the radionuclide records.

[8] In the following we will use the carbon cycle box model of *Köhler et al.* [2005a] to estimate the fraction of $\Delta^{14}C$ variability based on carbon cycle dynamics. We will first introduce the model and the temporal forcing used here over the last glacial cycle, and describe then how ^{14}C production rates were calculated from ^{10}Be or the geomagnetic field strength. We show simulation results of the global carbon cycle and compare reconstructed CO_2 with ice core data for the last 120 kyr. This will be followed by simulated changes in $\Delta^{14}C$ based on either constant or variable ^{14}C production rates. We discuss our simulation results with respect to the available $\Delta^{14}C$ data covering the last 50 kyr, but concentrate on the later half of this time window (26 kyr) due to the high uncertainties in the measurements. Our modeling approach is focused on glacial/interglacial variability. Therefore impacts on both atmospheric CO_2 and $\Delta^{14}C$ caused by a largely reduced THC in the Atlantic on a multicentennial to millennial timescale cannot be addressed straight forward with our model. However, its potential impacts on the carbon and ^{14}C cycle will be investigated in a detailed sensitivity analysis and discussed within the range of results coming from other studies.

2. Methods

2.1. Carbon Cycle Box Model BICYCLE

[9] BICYCLE is a global carbon cycle box model including a globally averaged atmospheric box and modules of the terrestrial and oceanic components of the carbon cycle (Figure 2). Carbon and the carbon isotopes ^{13}C and ^{14}C are prognostic variables of the model. Perturbations of the climate signals driving our model from the preindustrial situation are prescribed using available information obtained from various paleoclimatic records derived from ice cores and sediment records. The model descriptions of the terrestrial [*Köhler and Fischer*, 2004] and oceanic [*Köhler et al.*, 2005a] parts were published previously. The model was used recently to participate in the EPICA challenge as the most complex approach [*Wolff et al.*, 2004, 2005; *Köhler and Fischer*, 2006b] to propose variations in atmospheric CO_2 in the pre-Vostok period prior to the publication of the new EPICA Dome C CO_2 data [*Siegenthaler et al.*, 2005]. This application of BICYCLE on the long timescale of the EPICA challenge (740 kyr) shows that the process understanding gained from Termination I seems to be sufficient to reconstruct low-frequency changes in the global carbon cycle during the late Pleistocene. A downloadable version of the BICYCLE model is in preparation.

[10] It should be noted that carbon dioxide measured in ice cores is in general given as volume mixing ratio in parts per million by volume (ppmv), while carbon cycle models calculate the

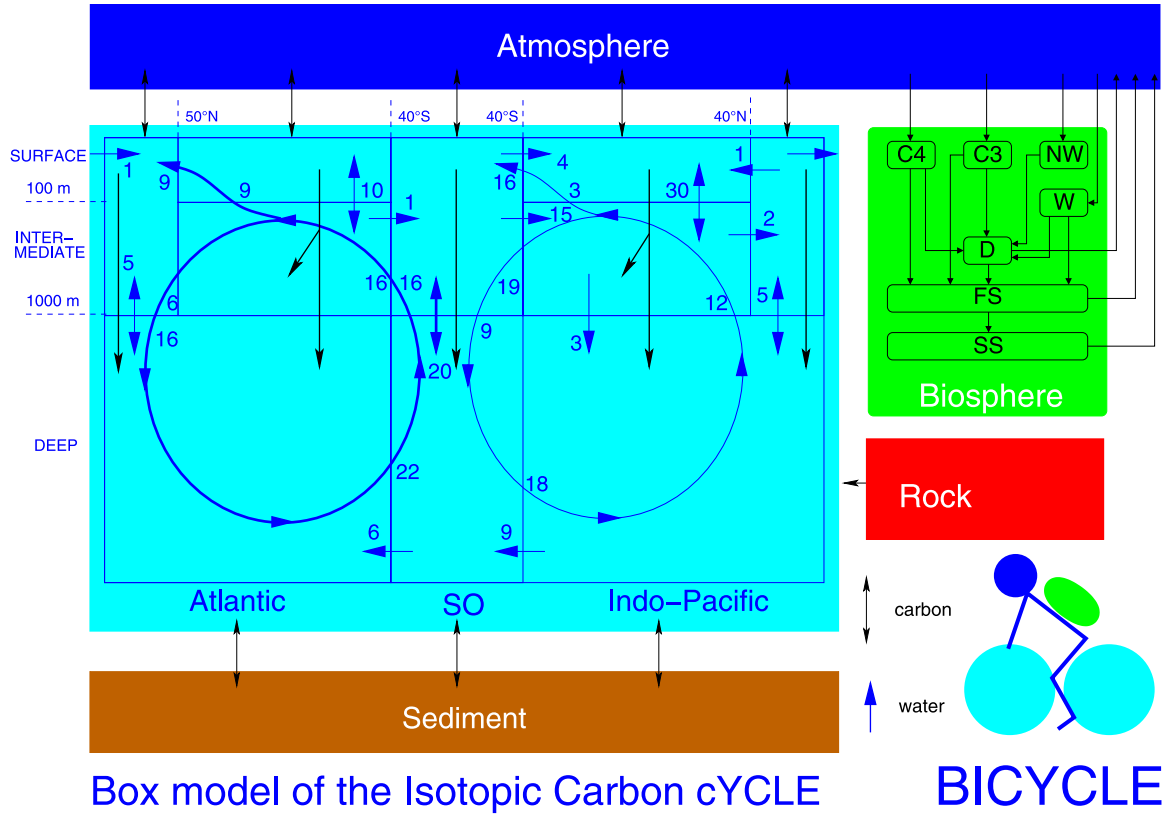

Figure 2. A sketch of the BICYCLE model including boundary conditions and preindustrial ocean circulation fluxes (in Sv = 10^6 m^2 s^{-1}) in the ocean module. Ocean circulation fluxes which change over time (NADW formation and subsequent fluxes, Southern Ocean vertical mixing) are depicted in bold arrows. The globally averaged terrestrial biosphere distinguishes ground vegetation following different photosynthetic pathways (C4, C3), nonwoody (NW), and woody (W) parts of trees, and soil compartments (D, FS, SS) with different turnover times.

atmospheric partial pressure (pCO_2 in μatm). Only in dry air and at standard pressure, they are numerically equal [*Zeebe and Wolf-Gladrow*, 2001]. For reasons of simplicity, we use throughout this article for both carbon dioxide data and simulation results the first nomenclature (CO_2 in ppmv) and assume equality between both. This simplification neglects a relatively constant offset between both quantities of a few ppmv.

2.2. Time-Dependent Forcing of the Model

[11] The model is perturbed from the preindustrial reference state by time-dependent boundary conditions based on various paleoclimatic records (Figure 3). Although the focus of this study is on the last 50 kyr (for which data-based reconstructions of atmospheric $\Delta^{14}C$ exists), we apply all forcings for a full glacial cycle of approximately 120 kyr in order to investigate how changes in the carbon cycle as seen in the atmospheric CO_2 records are covered with our modeling approach. We shortly introduce the paleoclimatic archives used here, but refer the reader interested in more details to earlier publications [*Köhler and Fischer*, 2004; *Köhler et al.*, 2005a]. The model is equilibrated for 3 kyr into a steady state (for 50 kyr if an increased ^{14}C production rates was assumed initially) for the environmental conditions found in 123 kyr BP and then run forward in time using the following time-dependent forcings. All paleoclimatic records were used on their individual age scales.

2.2.1. Sea Level

[12] We take the modeling results of *Bintanja et al.* [2005] for variations in sea level (Figure 3b). They are based on a compiled stack of 57 globally distributed benthic $\delta^{18}O$ records [*Lisiecki and Raymo*, 2005]. This approach neglects fast fluctuations caused by meltwater pulses.

2.2.2. Ocean Temperatures

[13] Ocean temperature changes are taken from isotopic temperature proxies as recorded in ice core

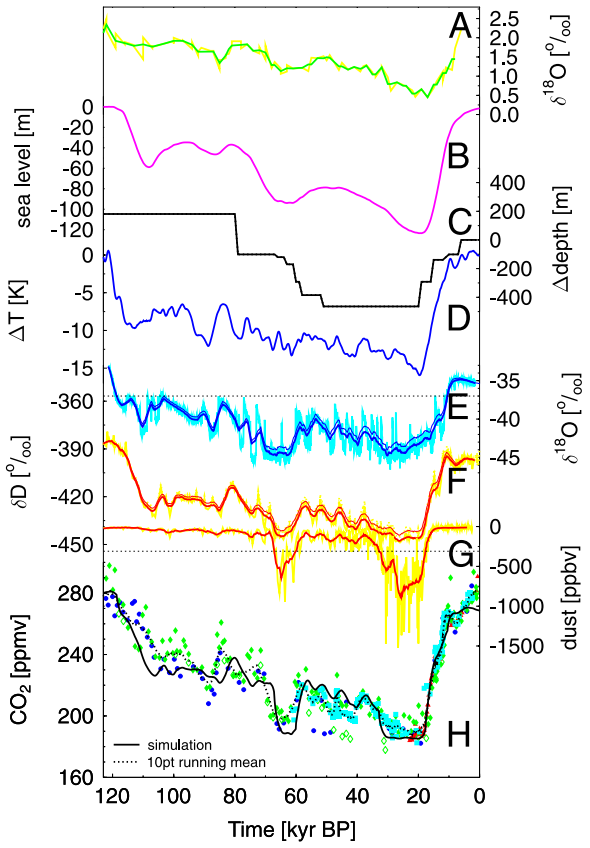

Figure 3. Paleoclimatic records which were used to force the BICYCLE model (Figures 3a–3g) and measured and simulated CO_2 (Figure 3h). (a) Planktic $\delta^{18}O$ of ODP677 [*Shackleton et al.*, 1990] (1°12′N, 83°44′W). (b) Changes in sea level [*Bintanja et al.*, 2005] based on stacked benthic $\delta^{18}O$ compiled by *Lisiecki and Raymo* [2005]. (c) Changes in the depth of the Pacific lysocline [*Farrell and Prell*, 1989]. (d) Changes in atmospheric temperature over land in the northern hemisphere (40–80°N) [*Bintanja et al.*, 2005]. (e and f) Original (thin) and sea level corrected (bold) $\delta^{18}O$ from (E) the Greenland ice core of NorthGRIP [*NorthGRIP Members*, 2004] and (f) the deuterium δD record from the Antarctic ice core at EPICA Dome C [*EPICA Community Members*, 2004]. (g) Atmospheric dust content as measured in the EPICA Dome C ice core [*EPICA Community Members*, 2004]. (h) Measured (points, 10 points running mean through all measurements: dashed line) and simulated (solid line) atmospheric CO_2. Data from Vostok (blue circles) [*Petit et al.*, 1999] plotted on the orbitally tuned age scale [*Shackleton*, 2000], Dome Fuji (green diamonds, open symbols: dry extraction, closed symbols: wet extraction techniques) [*Kawamura et al.*, 2003], Taylor Dome (cyan squares) [*Indermühle et al.*, 1999, 2000] on the timescale of *Brook et al.* [2000], EPICA Dome C (red triangles) [*Monnin et al.*, 2001, 2004]. Data prone to high-frequency fluctuations (Figures 3a, 3e, 3f, and 3g) were used as 3 kyr running means.

records drilled in neighboring continental ice sheets in the high latitudes and as recorded in planktic and benthic foraminifera for low latitudes and deep ocean boxes. For equatorial surface waters $\delta^{18}O$ data from ODP677 [*Shackleton et al.*, 1990] (1°12′N, 83°44′W) were taken to change SST scaled to a glacial/interglacial amplitude of 3.75 K [*Visser et al.*, 2003] (Figure 3a). Temperature changes in the intermediate and deep sea boxes are forced by data from *Labeyrie et al.* [1987] (not shown). Northern high-latitude SST were changed by $\delta^{18}O$ from the Greenland ice core NorthGRIP [*NorthGRIP Members*, 2004] (Figure 3e), while the Southern Ocean SST was forced by the deuterium δD record from the Antarctic EPICA Dome C ice core [*EPICA Community Members*, 2004] (Figure 3f). The two ice core temperature proxies were corrected for their embedded sea level change information [*Jouzel et al.*, 2003] and normalized to a glacial/interglacial amplitude in SST of 4 K [e.g., *Pflaumann et al.*, 2003; *Becquey and Gersonde*, 2003].

2.2.3. Gas Exchange Rates

[14] Changes in sea ice cover in the high latitudes will change the gas exchange rates there. Estimates of annual averaged sea ice cover change from their preindustrial 10×10^{12} m^2 in each hemisphere [*Cavalieri et al.*, 1997] to 14×10^{12} m^2 in the North and 22×10^{12} m^2 in the South [*Crosta et al.*, 1998a, 1998b; *Sarnthein et al.*, 2003; *Gersonde et al.*, 2005] are linearly coupled to variations in SST in the North Atlantic and Southern Ocean surface boxes in our model.

2.2.4. Ocean Circulation

[15] Measurements of the age difference between coexisting benthic and planktic foraminifera from western equatorial Pacific deep-sea cores suggest that the glacial overturning in the Pacific Ocean was comparable to the present-day situation [*Broecker et al.*, 2004]. Data- and model-based evidence, however, suggests a different circulation scheme in the Atlantic and the Southern Ocean during glacial times [e.g., *Meissner et al.*, 2003; *Hodell et al.*, 2003; *Knorr and Lohmann*, 2003; *McManus et al.*, 2004; *Watson and Naveira-Garabato*, 2006]. Glacial/interglacial changes in ocean circulation implemented in our scenarios are (1) a reduced glacial strength of the North Atlantic Deep Water (NADW) formation (10 Sv versus 16 Sv in preindustrial times), triggered by the North Atlantic SST proxy (glacial strength of NADW formation once $\delta^{18}O$ in NorthGRIP falls

below −37‰, Figure 3e), and (2) reduced glacial mixing in the Southern Ocean (31% of preindustrial exchange flux). The changes in the latter are linearly coupled to variation in SST in the Southern Ocean. Fluxes which change over time are depicted in bold blue arrows in Figure 2.

2.2.5. Iron Fertilization of the Marine Export Production

[16] In the preindustrial reference scenario, we prescribe an upper biological export production of organic matter at 100 m water depth of globally 10 PgC yr^{-1} [*Gnanadesikan et al.*, 2002] which is coupled via a constant rain ratio to the export of 1 PgC yr^{-1} of $CaCO_3$. This leads to un-utilized macro-nutrients in the Southern Ocean. In our model, these macro-nutrients are mobilized for the supply of additional export production once the dust concentration in the EPICA Dome C ice core [*EPICA Community Members*, 2004] (Figure 3g) exceeds 310 ppbv, a threshold which is deduced from carbon cycle dynamics seen during Termination I [*Köhler et al.*, 2005a]. Here, dust is an indirect proxy for the iron concentrations and forces the marine biota via the iron fertilization hypothesis [*Martin*, 1990; *Ridgwell*, 2003].

2.2.6. Terrestrial Carbon Storage

[17] Changes in the carbon storage in the terrestrial biosphere depend on the variations in the internal calculated CO_2 concentration and the global average temperature. The latter consists of a 3:1 mixture (representing the latitudinal distribution of land area excluding Antarctica) of hemispheric wide temperature estimates with amplitudes of 8 K in the North and 5 K in the South [*Kutzbach et al.*, 1998]. Here we take again the sea level corrected EPICA Dome C δD temperature proxy for the South [*EPICA Community Members*, 2004] (Figure 3f) and modeling results from *Bintanja et al.* [2005] for the North (Figure 3d). One example of an ensemble of possible forcing combinations was chosen here, when terrestrial carbon storage increases by more than 1000 PgC during the last glacial/interglacial transition, which is on the upper range proposed by other studies. The terrestrial module and scenarios with different amplitude of the glacial/interglacial change were analyzed elsewhere [*Köhler and Fischer*, 2004, 2006b].

2.2.7. $CaCO_3$ Chemistry

[18] All changes in the global carbon cycle lead to changes in the CO_3^{2-} ion concentration ($[CO_3^{2-}]$) in the deep ocean, which would then lead to variations in the sedimentation and dissolution rates of $CaCO_3$ and thus to fluxes of dissolved inorganic carbon (DIC) and alkalinity between the deep ocean and the sediments, a process known as carbonate compensation [*Broecker and Peng*, 1987]. In the absence of a process-based model of early diagenesis, which would calculate these fluxes, we prescribe the observed variations in the depth of the Pacific lysocline [*Farrell and Prell*, 1989] as another boundary condition (Figure 3c). The lysocline is the oceanic depth below which sedimentary calcite dissolves and is approximated here with the saturation depth of calcite, which is calculated as a function of depth (pressure) in vertical steps of 200 m and interpolated in-between. The lysocline in the Atlantic and Southern Ocean [*Crowley*, 1983; *Howard and Prell*, 1994] varied in its depth differently than in the Pacific, but sensitivity studies with our model [*Köhler and Fischer*, 2006a] have shown that these differences are of minor importance on the proposed atmospheric CO_2 and $\Delta^{14}C$ and are therefore neglected. From these additional boundary conditions the model generates DIC and alkalinity fluxes in order to bring changes in the simulated lysocline in line with the observations. This approach calculates net effects on the overall budgets of DIC and alkalinity and thus implicitly includes terrestrial weathering inputs of bicarbonate [*Munhoven*, 2002]. A data-based study [*Vecsei and Berger*, 2004] estimated that the growth of coral reefs during the last 20 kyr mainly occurred during the Holocene warm period and was especially restricted to times, in which the sea level was higher than 70 m below present. Its impact on the glacial/interglacial rise in CO_2 in the context of our model was investigated to be of minor importance and is neglected here. An approach which incorporates implicitly a temporal delay of the sedimentary response to changes in deep ocean $[CO_3^{2-}]$ as proposed by data and models [*Archer et al.*, 1997; *Marchitto et al.*, 2005] is used in an updated version of the model [*Köhler and Fischer*, 2006b]. The consequences of this improvement on carbon and ^{14}C are discussed in section 4.1.

2.3. Inferring Data-Based Information on the ^{14}C Production Changes

[19] Under the assumption that our knowledge on natural changes in the global carbon cycle has improved through the studies performed with the BICYCLE model, we can now calculate its implications on the ^{14}C cycle.

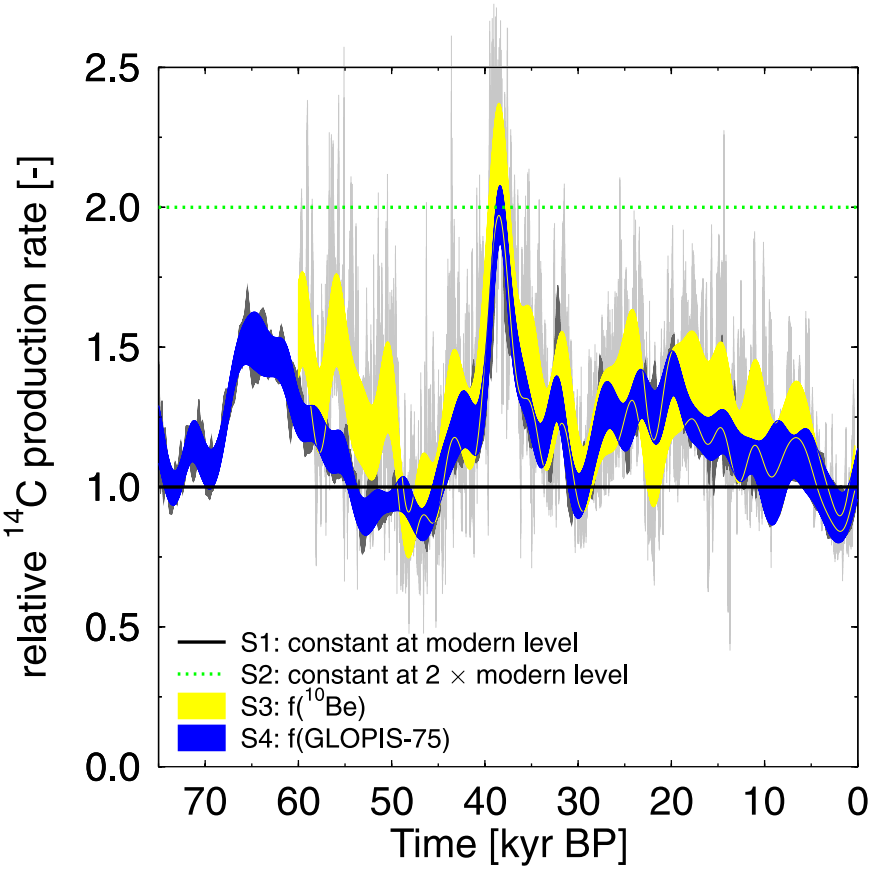

Figure 4. Time-dependent ^{14}C production rates as used in different simulation scenarios. Both the time-dependent ^{14}C production rates based on ^{10}Be and GLOPIS-75 are synchronized to the GRIP age scale. Shaded background shows the original data (light gray: area covered by lower and upper range based on ^{10}Be; dark gray: GLOPIS-75 (mean ±1 SD)) which are used for the simulations. Also plotted for clarity are a low-pass filtered version of the data sets (cutoff frequency = 1/3000 yr^{-1}) (yellow: ^{10}Be; blue: GLOPIS-75). The blue curve is overlayed on the yellow one. The thin yellow lines in the blue area mark the lower or upper end of the range based on ^{10}Be in the case of an overlap of the two curves.

[20] We first simulate carbon cycle dependent changes in atmospheric $\Delta^{14}C$ with BICYCLE based on constant ^{14}C production rates of either the modern level (scenario S1) or at twice the modern level (S2).

[21] A third scenario (S3) is based on inferred changes calculated from ^{10}Be measured at the GRIP and GISP2 ice cores [*Muscheler et al.*, 2004, 2005] covering the last 60 kyr (Figure 4). Finally, a recent high-resolution reconstruction of the geomagnetic field strength (GLOPIS-75) covering the last 75 kyr [*Laj et al.*, 2005] is taken as an alternative basis for the time-dependent changes in the ^{14}C production rates (S4). The ^{14}C production rates are calculated after *Masarik and Beer* [1999] using the normalized relative geomagnetic field strength. As described in *Muscheler et al.* [2004] the GISP2 timescale used for parts of the ^{10}Be record and originally for GLOPIS-75 was transferred to the GRIP timescale by synchronizing the $\delta^{18}O$ data sets of the GRIP and GISP2 ice cores.

[22] For both time-dependent approaches the range covered by either an lower and upper estimate (^{10}Be) or the standard deviation (GLOPIS-75) is used in our simulations. Two alternatives are proposed to analyze the importance of the initial ^{14}C production rates on the simulation results. First, the ^{14}C production rates between 123 kyr BP and the start of the reconstruction (60 kyr BP in S3; 75.8 kyr BP in S4) is set to modern values. This initial ^{14}C production rate is increased to 1.5 × modern values in a second set of experiments (S3x, S4x).

[23] For our simulations we use the original reconstructions of the relative ^{14}C production rates based on ^{10}Be and the GLOPIS-75 data sets, but for comparison and discussion a low-pass filtered version (cutoff frequency = 1/3000 yr^{-1}) is much more robust (Figure 4). GLOPIS-75 is based on a stack of 24 records, while the ^{10}Be-based records consists of the combined data sets from two ice cores. The short-term variability in the original data is larger in ^{10}Be than in the GLOPIS-75 record. The low-pass filtered reconstructions of the relative ^{14}C production rates vary between 0.8 and 2.4, but fluctuate most of the time between 1.0 and 1.5. They match each other remarkably well in the timing and the amplitude of the Laschamp event (~39 kyr BP at the GRIP ss09sea age scale), in which they rise to their maximum values of 2.0. Apart from one time window around 22 kyr BP the two reconstructions agree within their uncertainties or are larger if based on the ^{10}Be reconstruction than on the geomagnetic field. As discussed in detail by *Muscheler et al.* [2004], $\Delta^{14}C$ is very sensitive to small differences in the ^{14}C production rate. Long-term differences by 10% lead to modeled $\Delta^{14}C$ differences of 100‰.

[24] Regarding the ^{10}Be-based ^{14}C production rate, changes in climate could influence the ^{10}Be deposition and the assumption that it reflects global changes in the ^{14}C production rate could introduce errors. In the case of the geomagnetic-field based estimate of the ^{14}C production rate, it is possible that the choice and normalization of the included geomagnetic field records, long-term changes in solar activity or long-term changes in the galactic cosmic ray flux produce departures from the real history of the ^{14}C production rate. Therefore we use both approaches and a comparison of the results might give us information about possible biases in the assumed ^{14}C production rates.

2.4. Impact of Millennial-Scale Variability in the Ocean Circulation on the Carbon Cycle and on ^{14}C

[25] Various data- and model-based studies support the hypothesis that the ocean circulation, and here especially the North Atlantic Deep Water (NADW) formation was reduced during glacial times, and probably (nearly) completely shutdown during Heinrich events [e.g., *Rahmstorf*, 2002; *McManus et al.*, 2004]. In the more general interpretation of North-South teleconnection patterns with the concept of a bipolar seesaw each switch from an interstadial to a stadial period during millennial-scale climate oscillation of the Dansgaard/Oeschger events is connected with a reduced THC in the Atlantic Ocean [*Broecker*, 1998; *Stocker and Johnsen*, 2003; *Knutti et al.*, 2004; *EPICA Community Members*, 2006].

[26] In a forward model these millennial-scale variability in NADW formation can only be analyzed if especially the ice core records from Greenland and Antarctica are synchronized. Major improvements in this synchronization effort were made within the last years [e.g., *Blunier et al.*, 1998; *EPICA Community Members*, 2006], but so far the various records used here (especially NorthGRIP and EPICA Dome C) are taken on their individual timescales.

[27] We therefore analyze the impacts of abrupt changes in the northern deep water production on both atmospheric CO_2 and $\Delta^{14}C$ in a sensitivity study. We reduce the strength of the NADW formation (to a residual strength of 0, 2, 4, 6, or 8 Sv). Furthermore the length of the reduced overturning (500, 1000, 1500, 2000 years) and the ^{14}C production rates (constant at modern or 2 × modern level) are varied. It has to be noted that changes in NADW formation do not imply any additional changes in ocean temperature or sea ice formation. These processes are (in contrast to ocean general circulation models (OGCMs)) decoupled in our model. However, the marine export production is depending on nutrient availability in the surface waters and might be reduced during a reduced THC due to macro-nutrient depletion.

[28] We start these experiments from three different initial conditions. Two sets of experiments are performed for steady state background situations with all other processes held constant at their preindustrial level, no $CaCO_3$ exchange fluxes between deep ocean and sediment are considered here. The experiments differ only in the circulation scheme of the ocean, either an interglacial circulation as depicted in Figure 2 (NADW: 16 Sv; maximum net vertical mixing (20 Sv) in the Southern Ocean), or a glacial circulation (NADW: 10 Sv; minimum net vertical mixing (0 Sv) in the Southern Ocean). The third set of experiments is performed during transient simulations with all other processes which effect the carbon cycle active. The reduced strength of the NADW formation starts at 30 kyr BP. The chosen time period falls in a relatively stable climate period and corresponds approximately to the timing of the Heinrich 3 event [*Hemming*, 2004] and stadial 5

on the ss09sea timescale in the NorthGRIP and GRIP ice cores [*Dansgaard et al.*, 1993; *North-GRIP Members*, 2004].

3. Results

[29] Our approach to reinterpret observed atmospheric $\Delta^{14}C$ data is based on process understanding gained from the interpretation of the global carbon cycle. Dynamic variations in the carbon cycle as proposed by our model are therefore in our focus before we expand our interpretation to the ^{14}C cycle.

3.1. Carbon Cycle Reconstruction and Atmospheric CO_2

[30] In our standard simulation S1 over the last 123 kyr atmospheric CO_2 decreases gradually from its interglacial value of 280 ppmv before 120 kyr BP toward 230 ppmv around 105 kyr BP (Figures 3h and 5b). CO_2 then slowly decreases to 210 ppmv over most of the glacial period, before it sharply drops to its full glacial minima of 185 ppmv at 30 kyr BP. The slow decline is interrupted by millennial scale variability of up to 10 ppmv and a large negative excursion of 30 ppmv between 70 and 60 kyr BP. Between 18 and 10 kyr BP (Termination I) CO_2 rises by 85 ppmv within less than 10 kyr toward Holocene values. If compared with the available CO_2 data from Antarctic ice cores (Figure 3h), our simulation covers the low-frequency variations rather well (correlation of the simulation results and the 10-points running mean: $r^2 = 0.89$) while fast fluctuations during MIS 3 and the atmospheric rise in CO_2 in the late Holocene are not matched quantitatively in our experiment. Timing inconsistencies between our simulation results and the data during the glaciation and the peaks around 80 kyr BP (Figure 3h) might be due to the use of unsynchronized paleoclimatic records to force our model as mentioned in the section 2.2.

[31] The time-dependent contributions of eight processes to the rise in CO_2 are estimated by the difference from our standard simulation with experiments in which changes in the processes in question are switched off (Figure 5a). However, due to the high nonlinearity of the system this is only a first estimate, and all individual contributions derived by this method will not add up to the dynamics seen in the standard scenario. Changes in terrestrial carbon storage, sea level and sea ice are increasing glacial CO_2 by up to

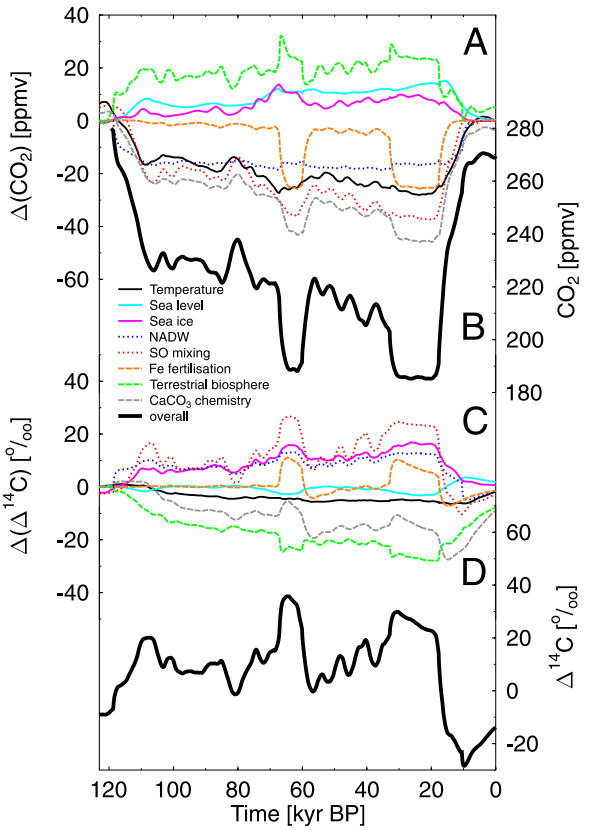

Figure 5. Simulation results for constant ^{14}C production rates (scenario S1). (a) Estimates of the individual contribution of different processes (ocean temperature, sea level, sea ice, NADW formation, Southern Ocean (SO) vertical mixing, iron (Fe) fertilization, terrestrial biosphere, $CaCO_3$ chemistry) on changes in atmospheric CO_2. Estimates are based on the differences of results of the standard scenario combining all processes and simulation with changes in all but the one process in question. (b) Transient dynamic of CO_2 in the standard scenario S1. (c and d) Same as in Figures 5a and 5b, but for atmospheric $\Delta^{14}C$.

10–20 ppmv each. Variations in the strength of the NADW formation contribute a rather constant 20 ppmv to the glacial reduction in CO_2, followed in amplitude by the effect of colder glacial ocean temperatures (25 ppmv). In the contribution of the latter, however, a gradual temporal increase in the CO_2 down-draw over time can be observed. Iron fertilization operates mainly during two peak windows, around 65 kyr BP and between 30 and 20 kyr BP, including the LGM, reducing CO_2 by about 25 ppmv. Southern Ocean mixing and the effect of processes acting on $CaCO_3$ follow very similar temporal pattern, with pronounced small millennial scale variability

and maximum amplitudes of 35 and 40 ppmv, respectively.

3.2. Variations in Atmospheric $\Delta^{14}C$ Based on Carbon Cycle Dynamics Under Constant ^{14}C Production Rates

[32] If we keep the ^{14}C production rate constant over time, we can now analyze which variations in atmospheric $\Delta^{14}C$ can be expected on the basis of changes in the global carbon cycle only. We can even further identify the temporal evolution of the contributions of different processes to the $\Delta^{14}C$ dynamics.

[33] The physical and the biological pump in the ocean bring carbon and ^{14}C from the surface to the deep ocean. Because of the two additional processes influencing ^{14}C (production in the atmosphere and radioactive decay), the vertical gradients in the ocean maintained by the oceanic pumps are different: DIC is enriched in the deep ocean and depleted at the surface while the opposite is the case for ^{14}C. A change in the strength of the pumps which are dominating both cycles therefore leads to opposing dynamics in atmospheric CO_2 and $\Delta^{14}C$: The overall dynamics of carbon cycle-based variations in $\Delta^{14}C$ calculated with constant ^{14}C production rates are in anti-phase with those seen in CO_2 (Figure 5d), e.g., atmospheric $\Delta^{14}C$ increases during times in which atmospheric CO_2 decreases and vice versa.

[34] Throughout most of the time of the last glacial cycles (110–20 kyr BP), $\Delta^{14}C$ is elevated by about 30‰ based on carbon cycle dynamics. This background increase is modulated by millennial scale variations of ±10‰ and punctuated by two periods with higher carbon cycle contributions (50–60‰) during a 10 kyr long window around 65 kyr BP and the period between 35 and 18 kyr BP including the LGM. However, the magnitude of these carbon cycle-based variations depends on the chosen modern ^{14}C production rate. If we double this production rate, for example, the carbon cycle-based $\Delta^{14}C$ variations increase to 110‰ during their maximum peaks (Figure 6). One has to note that in this scenario the background $\Delta^{14}C$ would rise to about 1000‰.

[35] Of course, the ^{14}C production rate cannot be arbitrarily chosen. The constraint on the ^{14}C production rate is that we can reproduce the preindustrial $\Delta^{14}C$ values. This can be achieved by normalizing the modeled $^{14}C/^{12}C$ ratios or by adjusting the absolute ^{14}C production rate to obtain

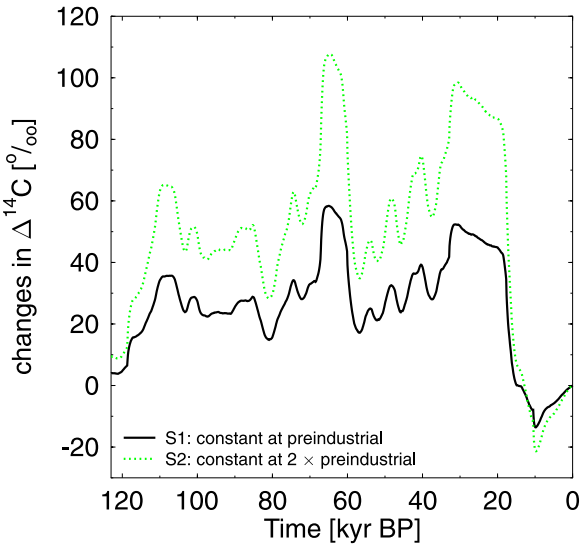

Figure 6. Carbon cycle-based changes in atmospheric $\Delta^{14}C$ based on different but constant ^{14}C production rates in scenarios S1 and S2.

the measured values. However, the discussion above shows that nonlinearities are an important aspect of our calculations. Due to the higher ^{14}C production rate during the last glacial [e.g., *Muscheler et al.*, 2004] the influence of the carbon cycle induced changes on $\Delta^{14}C$ at that time is expected to be larger than for the case of the relatively low modern ^{14}C production rate.

[36] The contribution of individual processes to the evolution in $\Delta^{14}C$ in scenario S1 with respect to the preindustrial time is estimated with the same approach as for CO_2 (subtracting results with the process of interest switched off from results of scenario S1). Again, this is a first order estimate which neglects nonlinearities and the individual contributions to $\Delta^{14}C$ (Figure 5c) will not sum up to the overall changes in $\Delta^{14}C$ seen in S1 (Figure 5d). SST and sea level do not impact on $\Delta^{14}C$. A reduced glacial terrestrial carbon storage and changes in the $CaCO_3$ chemistry lead to a reduction in $\Delta^{14}C$ by up to 25‰ each. The latter is caused by the dilution of the $\Delta^{14}C$ signal through the input of carbon depleted in ^{14}C entering the ocean/atmosphere/biosphere system from the sediments. The reduced glacial terrestrial carbon storage implies that oceanic glacial carbon reservoirs are increased. Due to the on average longer turnover time of carbon in the ocean compared to the terrestrial pools (in our model), more ^{14}C is taken up and removed for longer times from the atmosphere. The four remaining processes which all

Table 1. Sensitivity Study on the Effect of a Reduced NADW Formation on Atmospheric $\Delta^{14}C$ and CO_2[a]

	$\Delta(\Delta^{14}C)$, ‰, Modern ^{14}C Production Rates					$\Delta(\Delta^{14}C)$, ‰, 2 × Modern ^{14}C Production Rates					$\Delta(CO_2)$, ppmv				
	Residual NADW, Sv					Residual NADW, Sv					Residual NADW, Sv				
Length, years	0	2	4	6	8	0	2	4	6	8	0	2	4	6	8
Steady State, Interglacial Ocean Circulation															
500	17	15	13	11	9	33	29	26	22	17	−15	−15	−16	−16	−14
1000	21	18	15	13	10	43	37	31	26	21	−19	−18	−18	−18	−16
1500	24	20	16	13	11	48	40	33	27	22	−22	−19	−18	−18	−17
2000	25	20	16	13	11	51	41	33	27	22	−23	−19	−18	−18	−17
Steady State, Glacial Ocean Circulation															
500	32	25	18	11	5	65	51	36	23	11	−22	−18	−13	−8	−4
1000	42	35	24	14	6	85	70	48	29	13	−25	−25	−16	−9	−4
1500	47	39	26	15	7	95	79	52	31	14	−27	−28	−17	−10	−4
2000	50	41	27	15	7	100	83	54	31	14	−28	−29	−18	−10	−4
Transient, Start at 30 kyr BP															
500	29	24	19	13	7	58	48	37	27	13	−5	−4	−5	−6	−3
1000	41	33	24	17	9	82	66	49	34	17	−6	−6	−7	−8	−5
1500	47	37	27	19	9	96	75	54	37	19	−8	−8	−8	−9	−6
2000	52	39	28	19	10	105	80	56	38	19	−9	−8	−9	−10	−6

[a] Additionally to the strength of the residual NADW, the length of the experiment, the background ocean circulation and the constant ^{14}C production rates are varied. Maximal anomalies from initial values are summarized here.

increase glacial $\Delta^{14}C$ either restrict glacial gas exchange between the atmosphere and the surface ocean (sea ice: maximum contribution to $\Delta^{14}C \sim 20$‰), reduce the transport of water and thus ^{14}C from the surface to the deep ocean in glacial times (NADW formation: 15‰; Southern Ocean mixing 30‰), or impact on atmospheric $\Delta^{14}C$ through isotopic fractionation during higher marine export production caused by Fe fertilization leaving DIC enriched in ^{14}C in surface waters which would quickly enter the atmosphere through gas exchange (15‰).

[37] For twice as much ^{14}C production (scenario S2) the contribution of the individual processes is approximately doubled (not shown).

3.3. Millennial-Scale Variability of the Atlantic THC

[38] The anomalies in both atmospheric CO_2 and $\Delta^{14}C$ caused by a large decline in the NADW formation depend on all of the four chosen variables (residual strength of NADW, length of experiment, ^{14}C production rate, background conditions). The results of this sensitivity study are summarized in Table 1, some selected examples of simulated time series are shown in Figure 7. The simulated anomalies vary between −3 to −29 ppmv for atmospheric CO_2 and +5 and +105‰ for atmospheric $\Delta^{14}C$.

3.3.1. Atmospheric CO_2

[39] A reduced THC leads always to negative anomalies in atmospheric CO_2. Less carbon enriched deep water is transported to the surface in the Southern Ocean as a consequence of the reduced THC in the Atlantic Ocean.

[40] In experiments with large residual NADW (6–8 Sv) the anomalies in CO_2 are smaller in the glacial ocean than in the interglacial one. This different behavior between small and large residual NADW can be understood by the changing circulation patterns in the deep Atlantic Ocean. In all experiments a flux of 6 Sv is transporting water from the deep Southern Ocean to the deep Atlantic Ocean mimicking the Antarctic Bottom Water (AABW) (Figure 2). For experiments in which the residual NADW is larger than 6 Sv the resulting effect of NADW and AABW is still a net transport from the deep Atlantic to the deep Southern Ocean, while in experiments with smaller residual NADW the opposite is the case. In other words, the reduction in northern deep water production and thus the reduction in the subsequent upwelling of carbon-rich deep water in the Southern Ocean is

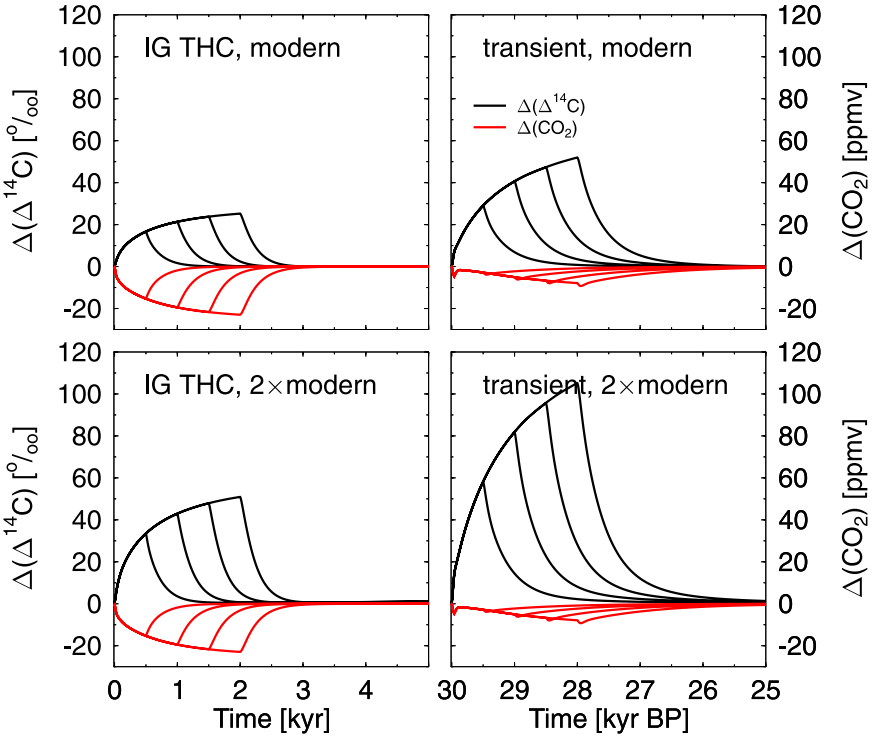

Figure 7. Examples for the effect of reduced northern deep water formation on atmospheric $\Delta^{14}C$ and CO_2. A complete shutdown of the NADW formation from either interglacial ocean circulation (IG THC) or transient experiments at 30 kyr BP with constant ^{14}C production rates (modern or 2 × modern level) was simulated. Four simulations with different length of the shutdown experiment (500, 1000, 1500, 2000 years) are shown.

smaller in the glacial than in the interglacial situation for the experiments with large residual NADW. For those experiments with small residual NADW upwelling in the Southern Ocean does not occur in the glacial ocean (net vertical mixing flux is reduced): no carbon-rich deep waters are entering the Southern Ocean surface box leading to larger drops in CO_2 than for the interglacial ocean, in which the deep Southern Ocean is ventilated via its vertical mixing rates. The glacial and the interglacial sets of experiments differ also in the amount in which the export production is reduced due to nutrient depletion. This reduction in marine export of carbon to the ocean interior depends also on the strength of the residual THC and is at maximum 16% in the glacial and 8% in the interglacial situation. A reduced export production leads to outgassing of CO_2 and counteracts the effect of the ocean circulation on the atmospheric CO_2.

[41] In the transient experiments the anomalies in CO_2 are reduced to a fourth to a half (residual NADW: 0–4 Sv) if compared to the glacial background conditions. This reduction of the initial anomalies is mainly caused by reduced marine export (at maximum reduced to a third during a complete THC shutdown) in combination with the negative feedback of the terrestrial biosphere via CO_2 fertilization: Lower CO_2 leads to less terrestrial photosynthesis, which is then followed by smaller terrestrial carbon storage and a rise in CO_2.

[42] The anomalies in CO_2 in the transient experiments are small, and additional contributions of other processes are expected. A largely reduced Atlantic THC would lead to a warming in the Southern Ocean [*Stocker and Johnsen*, 2003], which would then lead to outgassing of CO_2 due to a lower solubility of CO_2 in warm waters. The North Atlantic region and large parts of Eurasia would experience a cold period. This might lead to a southward migration of the treeline, a loss of carbon in the vegetation, but also to reduced respirational loss of carbon from the soil. During glacials the net effect would be a rise in CO_2 by up to 10 ppmv, however, the response depends on the background climate and might also be of opposite sign [*Köhler et al.*, 2005b]. In the marine biosphere, the North Atlantic plankton stocks might collapse and the export production of organic

carbon to the deep ocean might drop by 20% [*Schmittner*, 2005], which would then increase atmospheric CO_2. As a consequence of the bipolar temperature anomaly [*Stocker and Johnsen*, 2003], the sea ice cover in the North might rise while that in the South might shrink. As the North Atlantic is a sink to CO_2 while the Southern Ocean is a source, both sea ice anomalies would therefore lead to rising atmospheric CO_2 of a few ppmv. Terrestrial photosynthesis is directly dependent on the atmospheric concentration of carbon dioxide. Consequently, the effects of all these processes would not linearly add up to a combined effect but interact via existing feedbacks. Nevertheless, the order of magnitude deduced from these pieces of evidence agrees with the observed anomalies in CO_2 of +10–20 ppmv as seen between 60 and 30 kyr BP [*Indermühle et al.*, 2000], which could be explained by the combined effects initiated by a shutdown of the Atlantic THC [e.g., *Köhler et al.*, 2005b; *Schmittner*, 2005].

3.3.2. Atmospheric $\Delta^{14}C$

[43] The most important variable in this sensitivity study for the evolution of atmospheric $\Delta^{14}C$ is the residual strength of the NADW formation. A residual NADW of 8 Sv would imply that the THC is reduced only by 2 Sv in the glacial and in the transient experiment leading to a positive anomaly in $\Delta^{14}C$ of 5 to 20‰, while a complete shutdown of the NADW will result in +29 to +105‰. The less northern deep water is produced the more ^{14}C has to stay in the atmosphere.

[44] The size of the anomalies rise with the length of the reduction in northern deep water production. In the shortest experiments (500 years) simulating a complete shutdown only about a half to two thirds of the anomalies gained in the 2000 years experiments are found. This dependency on the length of the experiment is weaker if a larger residual northern deep water production (up to 8 Sv) is allowed.

[45] Twice the modern ^{14}C production rate leads also to approximately twice as large perturbations in $\Delta^{14}C$.

[46] For a small residual NADW (0–4 Sv) the impacts on atmospheric $\Delta^{14}C$ are smallest for interglacial ocean circulation, but the effects are twice as large if the experiments are started from either the glacial circulation or during the transient experiments. In experiments with larger residual NADW the effect of the ocean circulation is marginal.

[47] For the comparison of the interglacial and the glacial ocean circulation, the $\Delta^{14}C$ signal is tightly coupled to the carbon cycle and CO_2. If a similar reduction of the NADW in the glacial ocean leads to a larger (smaller) drop in CO_2 than in the interglacial ocean, a similar trend but with opposite sign is observed for $\Delta^{14}C$. A drop in CO_2 is caused by reduced upwelling of carbon-rich and ^{14}C-poor deep waters in the Southern Ocean. This process is more important for atmospheric CO_2 than the change in the deep water production and thus the downwelling of carbon in the North Atlantic itself, probably because of the four times larger areal extent of the Southern Ocean in our box model configuration. Deep waters are further enriched in carbon and depleted in ^{14}C in a glacial ocean with its reduced overturning compared to the interglacial situation. The loss of the upwelling deep waters through a complete shutdown of the THC in the Atlantic is therefore more important for the carbon and ^{14}C budgets at the surface in the glacial than in the interglacial climate.

[48] The situation is more difficult for the transient experiments. The anomalies in $\Delta^{14}C$ are similar to those obtained with glacial circulation, because the combined effect of the additional processes enriching $\Delta^{14}C$ at 30 kyr BP (sea ice, iron fertilization) compensate for the effects of those depleting $\Delta^{14}C$ at that time (terrestrial biosphere, $CaCO_3$ chemistry) (Figure 5c).

[49] The additional effects impacting on the carbon cycle which would follow a collapse of the Atlantic THC (bipolar anomalies of temperature and sea ice, marine and terrestrial biology) have also to be considered for the ^{14}C cycle. Temperature changes are of minor importance for ^{14}C, the opposing sea ice anomalies in both hemispheres might lead to a neglecting effect, and the reduced photosynthesis in both the marine and terrestrial biosphere would lead to a slight damping of the $\Delta^{14}C$ anomalies.

[50] We conclude that a complete shutdown of the NADW formation might at maximum lead to a peak of +100‰ in $\Delta^{14}C$. However, realistic ^{14}C production rates were usually smaller than the 2 × modern values needed to achieve this result. A further damping of the amplitude would be caused by the expected changes in the biospheric response to the THC collapse. Therefore, on the basis of our model understanding, amplitudes of up 50‰ seemed to be realistic. These results are in line

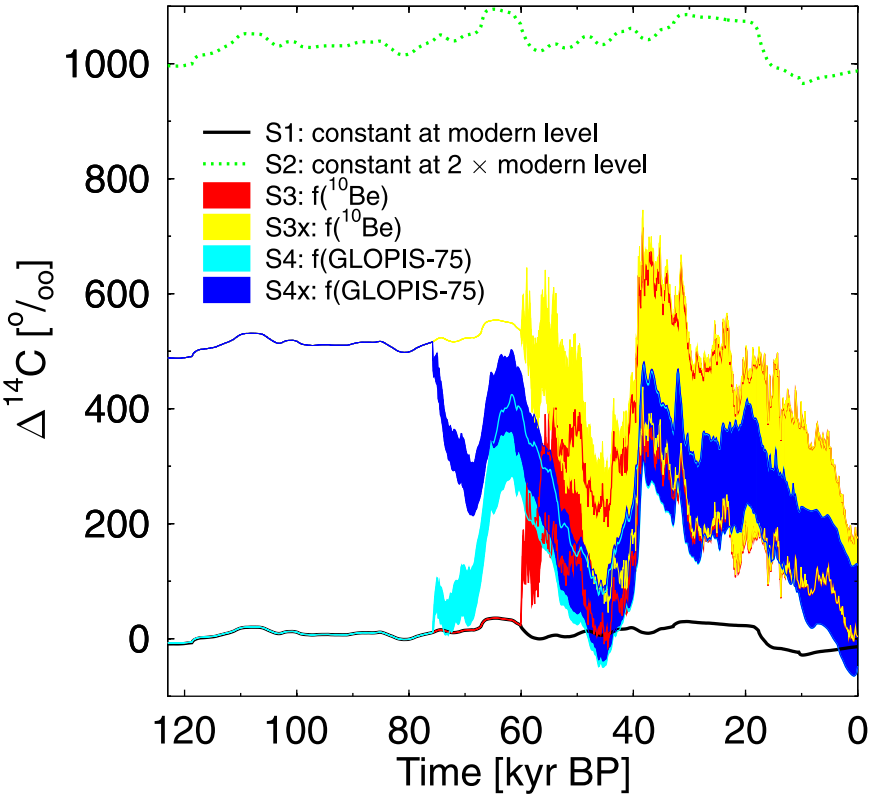

Figure 8. Simulated atmospheric $\Delta^{14}C$ based on different ^{14}C production rates. Simulations S3 and S4 are initialized with modern ^{14}C production rates; S3x and S4x are initialized with 1.5 × modern ^{14}C production rates. The results of the four scenarios S3, S3x, S4, and S4x span wider ranges because of the uncertainties in the time-dependent ^{14}C production rates shown in Figure 4. Curves are overlayed on each other (S4x on top of S4, S3x on top of S3, both S4 and S4x on top of S3 and S3x). Upper and lower ends of the ranges of the underlying curves are then indicated by the thin lines.

with those received recently with an OGCM. In a freshwater perturbation experiment, *Butzin et al.* [2005] reduced the NADW export at 30°S from 9 Sv to 1 Sv which led to a rise in atmospheric $\Delta^{14}C$ of 40‰.

[51] A reduced NADW formation would also lead to positive anomalies in atmospheric $\delta^{13}C$ of CO_2. This $\delta^{13}C$ record derived from ice cores [*Smith et al.*, 1999] is only coarsely resolved and is only going back in time as far as 26 kyr BP. However, the $\delta^{13}C$ signal indicates that during the Younger Dryas cold event, also known as stadial 1, (~12.7 to 11.5 kyr BP) the NADW formation was not largely reduced [*Köhler et al.*, 2005a, 2006].

3.4. Impact of Time-Dependent ^{14}C Production Rates

[52] The initial ^{14}C production rate significantly affects $\Delta^{14}C$ for the first 20 kyr in which the ^{14}C production varies (Figure 8). This conclusion can be drawn from both the comparisons of the scenarios driven by ^{10}Be (S3, S3x) and those driven by the geomagnetic field (S4, S4x). The ^{10}Be record and thus the variable ^{14}C production rates cover the last 60 kyr BP, while the geomagnetic field reconstruction goes 75 kyr back in time. Simulations S3 and S3x therefore differ by 500‰ for constant ^{14}C production rates (before 60 kyr BP), converge between 60 and 40 kyr BP, and are nearly identical thereafter. The same is happening for S4 and S4x 15 kyr earlier (500‰ difference before 75 kyr BP, converging between 75 to 55 kyr BP, nearly identical thereafter). This initial effect has to be kept in mind if simulation results are compared with data-based reconstructions.

[53] The range of the simulated $\Delta^{14}C$ based on ^{10}Be is about 300‰ wide at 50 kyr BP, which is reduced to 200‰ for recent times (Figure 9). The ^{10}Be-based range of variability is inferred from different combinations of the ^{10}Be data from the GRIP and GISP2 ice core. Due to the reservoir effect and the ^{14}C decay $\Delta^{14}C$ decreases caused by a diminished ^{14}C production rate are relatively

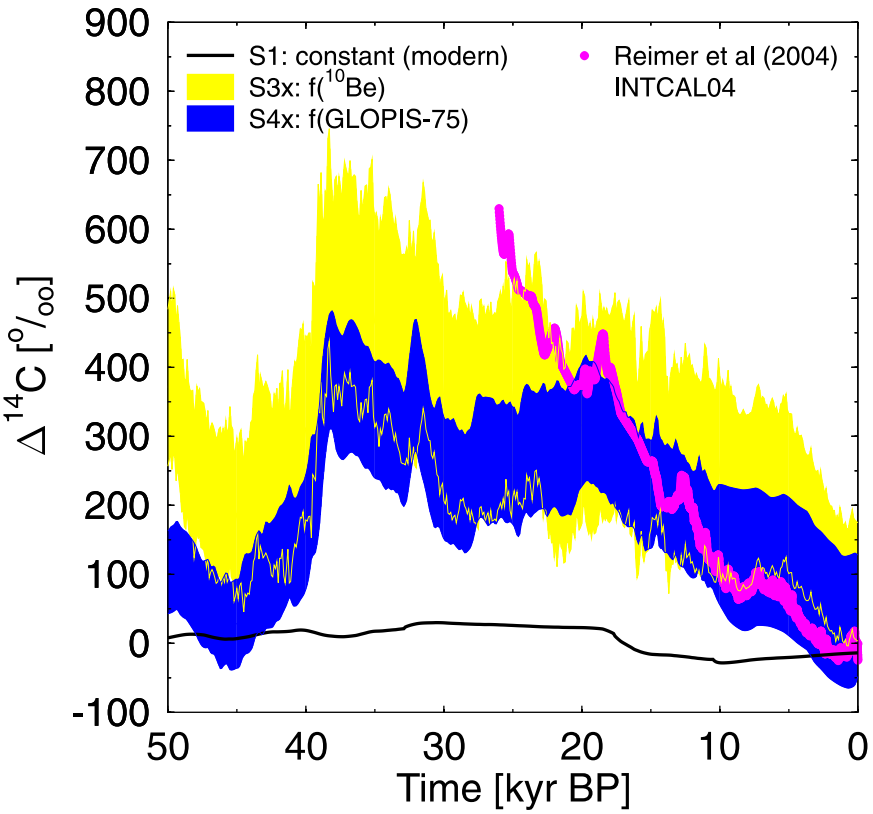

Figure 9. Comparison of the simulated atmospheric $\Delta^{14}C$ based on different ^{14}C production rates during the past 50 kyr with the INTCAL04 data set [*Reimer et al.*, 2004]. The results of the scenarios S3x and S4x span wider ranges because of the uncertainties in the time-dependent ^{14}C production rates shown in Figure 4. Curves are overlayed on each other (S4x on top of S3x). Upper and lower ends of the ranges of the underlying S3x are then indicated by the thin yellow lines.

slow [*Muscheler et al.*, 2004]. This means that the climate system cannot transfer within a short period of time from a state with atmospheric $\Delta^{14}C$ at the upper end of the range given by the uncertainty of the ^{10}Be-based ^{14}C production rate to a state with $\Delta^{14}C$ at the lower end of this range. In other words, even if the $\Delta^{14}C$ error range comprises 300‰, the ^{10}Be-based ^{14}C production rate cannot explain most of the steep $\Delta^{14}C$ decrease during the last deglaciation.

[54] The smaller uncertainty in the ^{14}C production rates based on GLOPIS-75 leads to $\Delta^{14}C$ results with uncertainties of only ~200‰ throughout the last 50 kyr. In both simulations (S3, S4) atmospheric $\Delta^{14}C$ declines by ~400‰ over the last 38 kyr. The lowest GLOPIS-75-based $\Delta^{14}C$ values are for most of the simulation time about 100‰ lower than the range covered by ^{10}Be-based scenarios. For the time period 50 kyr BP to 16 kyr BP the scatter in the atmospheric $\Delta^{14}C$ data is still large (Figure 1). For reasons of simplicity we compare our simulation results only with the INTCAL04 record going 26 kyr back in time [*Reimer et al.*, 2004] (Figure 9). The large variability spanned by our simulation results over the last 50 kyr is in agreement with the variability found in the data sets, only certain data sets with $\Delta^{14}C$ larger than 700‰ fall out of the range obtained by our results (e.g., *Beck et al.* [2001], prior to 35 kyr BP). The GLOPIS-75-based scenario is not covering the INTCAL04 data within its uncertainty range prior to 15 kyr BP, while the ^{10}Be-based scenario is underestimating atmospheric $\Delta^{14}C$ only for the earliest part (26–24 kyr BP). After 10 kyr BP the general trend seen in $\Delta^{14}C$ in INTCAL04 is covered by the simulations based on GLOPIS-75, while those based on ^{10}Be are slightly higher than the data set. The general trend of a reduction in atmospheric $\Delta^{14}C$ seen in the data sets is covered by our scenarios, however, the gradient of ~500‰ over the last 30 kyr is not covered in any of our scenarios.

[55] Millennial-scale climate variability caused by a reduced Atlantic THC might be responsible for the sharp positive anomalies seen in the $\Delta^{14}C$ data sets (e.g., of +50 to +100‰ at 12.5, 18.5, 22 kyr BP in INTCAL04). These changes in ocean circulation are generally assumed to have been taken place during interstadial/stadial climate transitions, especially during the beginning of the Younger Dryas or Heinrich events [e.g., *Stocker and Johnsen*, 2003; *EPICA Community Members*, 2006], they might also be caused by meltwater pulses [*Clark et al.*, 2002]. According to our model and the study of *Butzin et al.* [2005] peaks up to approximately 50‰ might be caused by reduced northern deep water production. However, while the peak at 12.5 kyr BP might fall together with the onset of the Younger Dryas, those at 18.5 and 22 kyr are not connected with stadial climate conditions seen in Greenland ice cores [e.g., *NorthGRIP Members*, 2004] or a known Heinrich event. According to *Hemming* [2004] Heinrich events 1 (16.8 kyr BP) and 2 (24 kyr BP) were about 2 kyr earlier respectively later than these $\Delta^{14}C$ anomalies. While the peak at 18.5 kyr BP falls together with an abrupt rise in sea level and thus a meltwater pulse at 19 kyr BP [*Clark et al.*, 2004], which might nevertheless indicate a change in the Atlantic THC as cause for this anomaly, similar details on sea level and subsequent changes in the THC are not retrievable for the peak at 22 kyr BP. All highly resolved reconstructions of sea level during Termination I are based on coral reef terraces and start not before 22 kyr BP [*Lambeck and Chappell*, 2001].

4. Discussion and Conclusions

[56] In this study we combined proxy-based information on the ^{14}C production rates with simulation results of the global carbon cycle box model BICYCLE to interpret the observed atmospheric $\Delta^{14}C$ data during the last 50 kyr. To deepen this interpretation we discuss in the following the model limitations of BICYCLE (section 4.1), and compare our results on $\Delta^{14}C$ with other studies (section 4.2), before we end with our final conclusions (section 4.3).

4.1. Model Limitations and the Global Carbon Cycle

[57] Our approach is based on a simple global carbon cycle model. We are therefore able to force our model externally with available proxy data and to run it over hundreds of thousands of years in a reasonable computing time. The more complex a model gets (i.e., in terms of spatial resolution) the more difficult it gets to find appropriate paleoclimatic archives to force it forward in time. This simplicity restricts also the kind of processes which are included in the model in an accurate way. However, the natural variability in the global carbon cycle on glacial/interglacial time scales is covered with our model. We can at least propose a scenario which is plausible and in line with various pieces of evidence from different archives. The same processes as in our simulations have to be at least considered in other simulation scenarios to explain the glacial/interglacial CO_2 rise, but the quantitative contributions of individual processes may differ (see more detailed discussion by *Köhler et al.* [2005a]). More complex scenarios such as the "silicic acid leakage hypothesis" [*Matsumoto et al.*, 2002], which involves a time-dependent and spatial heterogenous change in the distribution of nutrients, species composition and export of organic and inorganic matter, cannot be followed up in details with our model.

[58] For the Holocene we did not implement recent theories which try to explain the rise in CO_2 by 20 ppmv during the last 8 kyr [*Indermühle et al.*, 1999], and therefore our simulation results do not match the CO_2 data very well. It should be mentioned that these theories are so far not mutually exclusive, but each idea follows different data or model constraints [e.g., *Broecker and Clark*, 2003; *Ridgwell et al.*, 2003; *Ruddiman*, 2003; *Joos et al.*, 2004].

[59] It should be noted that our simulation results propose a contribution of an increased glacial marine export production to the higher glacial atmospheric $\Delta^{14}C$ due to Fe fertilization in the Southern Ocean. This change in the global carbon cycle leads to a 20 ppmv reduction in CO_2 and is in the range estimated from sediment cores [*Kohfeld et al.*, 2005]. Furthermore, it has been argued on the basis of the understanding which emerged from present day Fe fertilization experiments that the contribution of this process to the glacial decline in CO_2 is probably less than 1 ppmv and at maximum 14 ppmv [*de Baar et al.*, 2005]. However, these conclusions were based on a study of dust and iron fluxes to Antarctica in which the glacial flux was 11-fold larger than at present [*Edwards et al.*, 1998]. Recent iron flux studies from the EPICA Dome C ice core [*Gaspari et al.*, 2006; *Wolff et al.*, 2006] find a 25- to 34-fold increase in glacial iron flux to Antarctica. This would rise the upper limit

of the impact of Fe fertilization as given by *de Baar et al.* [2005] by more than a factor of two, and we thus would find our simulation results in a range possible from the observations.

[60] To base the carbonate compensation mechanism on changes in the lysocline as done here bears also the uncertainties contained in the reconstruction of the Pacific lysocline. *Archer* [1991] posed the question if the lysocline data of *Farrell and Prell* [1989] record more a production or a dissolution signal and raised also concerns that there might be a latitudinal bias in the data. This lysocline approach leads also to a more or less instantaneous response of the carbonate compensation to changes in deep ocean [CO_3^{2-}], while process-based models of early diagenesis [*Archer et al.*, 1997] and paleo records [*Marchitto et al.*, 2005] indicate that this process is time-delayed with a response time which can be approximated with an e-folding time τ of 1.5 to 6 kyr. In an updated version of the model which takes this temporal delay into account [*Köhler and Fischer*, 2006b] the contribution of the $CaCO_3$ chemistry to changes in atmospheric CO_2 is about half as large as here (τ = 1.5 kyr) and the correlation between simulation results and CO_2 data over the last 650 kyr is slightly smaller (r^2 = 0.75). This different behavior of the carbon cycle might also reduce the contribution of the $CaCO_3$ chemistry to $\Delta^{14}C$ by up to a factor of two. The updated model version [*Köhler and Fischer*, 2006b] considers also a by a factor of two smaller glacial/interglacial change in the terrestrial carbon storage (500 PgC), which is at the lower end of the range covered by data- and model-based studies [*Köhler and Fischer*, 2004]. This would also reduce the impact of terrestrial processes on atmospheric $\Delta^{14}C$. The uncertainties within these two processes taken together imply that the overall carbon-based influence on atmospheric $\Delta^{14}C$ might be up to 30‰ higher in a simulation with the updated model than in scenario S1.

4.2. Comparison of Our Interpretation of $\Delta^{14}C$ With Other Modeling Studies

[61] If we compare our results with other approaches to reconstruct atmospheric $\Delta^{14}C$ [*Beck et al.*, 2001; *Hughen et al.*, 2004] some similarities and some differences become apparent. *Beck et al.* [2001] used a similar multi-box model and combined a few assumptions to match their simulation results to their own observations covering 45–10 kyr BP. According to their study the long-term decline in $\Delta^{14}C$ can be explained by changes in the ^{14}C production rates, an increase in carbonate sedimentation rates by one order of magnitude and a gradually increase in the THC from 35 to 11 kyr BP. In *Hughen et al.* [2004] an even simpler model was applied consisting of seven boxes only. Again several assumptions on changes in ^{14}C production rate, ocean circulation and carbonate sedimentation are combined to be able to explain the long-term dynamics seen in the $\Delta^{14}C$ observations. With 100‰ the amplitude in $\Delta^{14}C$ caused by changes in the THC is in both studies larger than in our scenarios. We calculate a contribution of 45‰ for changes in ocean circulation under constant modern ^{14}C production rates. If we assume a rise in the glacial ^{14}C production rate by 50% this would enlarge the THC contribution to about 70‰. Interestingly, changes in the gas exchange rates (sea ice) and the marine export production have also important impacts on atmospheric $\Delta^{14}C$ in our model while these processes were not considered in the other two studies.

[62] Similar to *Beck et al.* [2001], the sedimentation rates proposed by our model rise also over Termination I. Our approach of simulating $CaCO_3$ chemistry considers only the net changes between terrestrial weathering inputs and losses to the sediments. The simulated ocean/atmosphere/biosphere system is about 2000 PgC smaller in carbon during interglacial times than during the LGM [*Köhler and Fischer*, 2006a]. This decline of the total active carbon pools in ocean, atmosphere, and biosphere leads to lower $\Delta^{14}C$ (−20‰ at modern ^{14}C production rates) between 35 and 15 kyr BP followed by a rising contribution to $\Delta^{14}C$ thereafter (Figure 5c). While the declining trend is also seen in *Beck et al.* [2001], its contribution to glacial $\Delta^{14}C$ is an order of magnitude larger in their study (−300‰). Changes in the shallow water sedimentation rates over Termination I were also important in *Hughen et al.* [2004] accounting for a decline of 150‰ in $\Delta^{14}C$. *Beck et al.* [2001] assume a rise in sedimentation rates from 0.24 PgC yr^{-1} until 25 kyr BP to 2.0 PgC yr^{-1} at 11 kyr BP, identical to a loss of 15,680 PgC to the sediments, but they give no information about assumed weathering rates. In *Hughen et al.* [2004] the preindustrial ocean is losing as much carbon to the sediments as it gains from the continental weathering. In the reduced glacial carbon cycle assumed by *Hughen et al.* [2004] the losses to the sediments are approximately half as large as the gain from weathering. This rise in the sedimentation rates from glacial to interglacial conditions would also lead to a loss of carbon of the order of 5,000–10,000 PgC (depending on the assumed temporal evolution). In all three studies

(Beck, Hughen, this study) the amount of ^{14}C contained in both the weathering inputs and the sedimentation and dissolution of $CaCO_3$ might be important for the budgets. Since these numbers are not given in the other studies their importance on the results cannot be assessed, however, we tested the effect of the ^{14}C content of these fluxes on atmospheric $\Delta^{14}C$ within our modeling framework. In our study the $\Delta^{14}C$ of sedimented $CaCO_3$ is similar to that during production in the surface ocean, while the ^{14}C of dissolved $CaCO_3$ might vary due to its residence time in the sediments. A variation of ^{14}C of this dissolution flux between that of newly built sediments and old sediments without any ^{14}C revealed only slight changes in our overall simulation results. Therefore the amount of carbon which is extracted from the ocean to the sediments in a glacial/interglacial transition is most important for the ^{14}C. However, its variability is large between the three studies (2,000 to 16,000 PgC), but difficult to assess without additional information such as carbon cycle dynamics and impacts on atmospheric CO_2.

[63] The choice on which approach the ^{14}C production rate is based on is a very important assumption for the ability of a case study to reconstruct the observed decline in atmospheric $\Delta^{14}C$ during the last 30 kyr. In a previous study applying the BICYCLE model over Termination I [*Köhler et al.*, 2005a], we used a record of the geomagnetic field strength based on NAPIS-75 [*Laj et al.*, 2002] to reconstruct changes in the ^{14}C production rates. A remarkable better fit of the simulated $\Delta^{14}C$ to the data-based reconstruction was achieved. The main difference between NAPIS-75 and GLOPIS-75 is that NAPIS-75 produces higher ^{14}C production rates between 30 and 20 kyr BP and contains therefore a larger negative gradient over the last 20 kyr. As a result simulated $\Delta^{14}C$ based on NAPIS-75 would be higher than those based on GLOPIS-75 at 30 kyr BP and decrease faster bringing the simulations better in line with the observations. NAPIS-75 was also used by *Hughen et al.* [2004], while the study of *Beck et al.* [2001] is based on SINT200, a similar geomagnetic stack with high uncertainty and very low temporal resolution. The chosen ^{14}C production rate is also important for the conclusions of *Robinson et al.* [2005]. They attributed the difference between the solely production-driven variability (based on ^{10}Be) and the reconstruction in atmospheric $\Delta^{14}C$ between 26 and 10 kyr BP to changes in the carbon cycle, mainly to changes in ocean circulation.

[64] We challenge our model also to reconstruct atmospheric CO_2 and base our assumptions how the carbon cycle might have varied over time as much as possible on data constraints. A similar cross-check of the simulations results was not performed in the other studies, but this would help to assess the results of their studies.

4.3. Conclusions

[65] We have proposed in this study that the changes in the ^{14}C production rate have a dominant influence on the $\Delta^{14}C$ record. According to our model a changing carbon cycle during glacial times contributes with less than 100‰ about a 1/6 to the observed atmospheric $\Delta^{14}C$ variability during the last 50 kyr. Glacial atmospheric $\Delta^{14}C$ larger than 700‰ cannot not be explained within our framework, neither through carbon cycle-based changes nor through variable ^{14}C production. It is not clear which processes might be responsible for these observations. An assumed shutdown of the NADW formation which might have occurred during stadial climate conditions and especially Heinrich events might lead to positive anomalies of ~50‰ in $\Delta^{14}C$. Our proposed scenario is in line with observed atmospheric CO_2. A further constraint for its plausibility might come from a comparison of simulated and measured atmospheric $\delta^{13}C$, a new ice core record which is urgently wanted in high precision and good temporal resolution for a better understanding of the global carbon cycle [e.g., *Broecker and Stocker*, 2006].

Acknowledgments

[66] We thank Kenji Kawamura for the Dome Fuji CO_2 data, Richard Bintanja for the sea level and temperature change data, and Catherine Kissel and Carlo Laj for the GLOPIS-75 record. We also thank Laurent Labeyrie, Jean Lynch-Stieglitz, Tzu-Chien Chiu, and an anonymous reviewer for their constructive comments, which helped shift the focus of this study and improved its quality. P.K. and H.F. were funded by the German Ministry of Education and Research through project RESPIC of the German Climate Research Programme (DEKLIM). This study was in part sponsored by the Swiss National Science Foundation, NSF, and NASA (RM).

References

Archer, D., H. Kheshgi, and E. Maier-Reimer (1997), Multiple timescales for neutralization of fossil fuel CO_2, *Geophys. Res. Lett.*, *24*, 405–408.

Archer, D., A. Winguth, D. Lea, and N. Mahowald (2000), What caused the glacial/interglacial atmospheric pCO_2 cycles?, *Rev. Geophys.*, *38*(2), 159–189.

Archer, D. E. (1991), Equatorial Pacific calcite preservation cycles: Production or dissolution?, *Paleoceanography*, *6*, 561–571.

Bard, E., M. Arnold, B. Hamelin, N. Tisnerat-Laborde, and G. Cabioch (1998), Radiocarbon calibration by means of mass spectrometric $^{230}Th/^{234}U$ and ^{14}C ages of corals: An update data base including samples from Barbados, Mururoa and Tahiti, *Radiocarbon*, *40*, 1085–1092.

Beck, J. W., et al. (2001), Extremely large variations of atmospheric ^{14}C concentration during the Last Glacial Period, *Science*, *292*, 2453–2458.

Becquey, S., and R. Gersonde (2003), A 0.55-Ma paleotemperature record from the Subantarctic zone: Implications for Antarctic Circumpolar Current development, *Paleoceanography*, *18*(1), 1014, doi:10.1029/2000PA000576.

Beer, J., et al. (1990), Use of ^{10}Be in polar ice to trace the 11-year cycle of solar activity, *Nature*, *347*, 164–166.

Bintanja, R., R. van der Wal, and J. Oerlemans (2005), Modelled atmospheric temperatures and global sea levels over the past million years, *Nature*, *437*, 125–128, doi:10.1038/nature03975.

Blunier, T., et al. (1998), Asynchrony of Antarctic and Greenland climate change during the last glacial period, *Nature*, *394*, 739–743.

Broecker, W., S. Barker, E. Clark, I. Hajdas, G. Bonani, and L. Stott (2004), Ventilation of the glacial deep Pacific Ocean, *Science*, *306*, 1169–1172.

Broecker, W. S. (1998), Paleocean circulation during the last glaciation: A bipolar seesaw?, *Paleoceanography*, *13*(2), 119–121.

Broecker, W. S., and E. Clark (2003), Holocene atmospheric CO_2 increase as viewed from the seafloor, *Global Biogeochem. Cycles*, *17*(2), 1052, doi:10.1029/2002GB001985.

Broecker, W. S., and T.-H. Peng (1987), The role of $CaCO_3$ compensation in the glacial to interglacial atmospheric CO_2 change, *Global Biogeochem. Cycles*, *1*, 15–29.

Broecker, W. S., and T. F. Stocker (2006), The Holocene CO_2 rise: Anthropogenic or natural?, *Eos Trans. AGU*, *87*, 27.

Brook, E. J., S. Harder, J. Severinghaus, E. J. Steig, and C. M. Sucher (2000), On the origin and timing of rapid changes in atmospheric methane during the last glacial period, *Global Biogeochem. Cycles*, *14*, 559–572.

Butzin, M., M. Prange, and G. Lohmann (2005), Radiocarbon simulations for the glacial ocean: The effects of wind stress, Southern Ocean sea ice and Heinrich events, *Earth Planet. Sci. Lett.*, *235*, 45–61.

Cavalieri, D. J., P. Gloersen, C. L. Parkinson, J. C. Comiso, and H. J. Zwally (1997), Observed hemispheric asymmetry in global sea ice changes, *Science*, *278*, 1104–1106.

Clark, P. U., N. G. Pisias, T. F. Stocker, and A. J. Weaver (2002), The role of the thermohaline circulation in abrupt climate change, *Nature*, *415*, 863–869.

Clark, P. U., A. M. McCabe, A. C. Mix, and A. J. Weaver (2004), Rapid rise of sea level 19,000 years ago and its global implications, *Science*, *304*, 1141–1144.

Crosta, X., J.-J. Pichon, and L. H. Burckle (1998a), Application of modern analog technique to marine Antarctic diatoms: Reconstruction of maximum sea-ice extent at the Last Glacial Maximum, *Paleoceanography*, *13*, 284–297.

Crosta, X., J.-J. Pichon, and L. H. Burckle (1998b), Reappraisal of Antarctic seasonal sea-ice extent at the Last Glacial Maximum, *Geophys. Res. Lett.*, *14*, 2703–2706.

Crowley, T. J. (1983), Calcium-carbonate preservation patterns in the central North Atlantic during the last 150,000 years, *Mar. Geol.*, *51*, 1–14.

Dansgaard, W., et al. (1993), Evidence for general instability of past climate from a 250-kyr ice-core record, *Nature*, *364*, 218–220.

de Baar, H. J. W., et al. (2005), Synthesis of iron fertilization experiments: From the Iron Age in the Age of Enlightenment, *J. Geophys. Res.*, *110*, C09S16, doi:10.1029/2004JC002601.

Delaygue, G., T. Stocker, F. Joos, and G.-K. Plattner (2003), Simulation of atmospheric radiocarbon during abrupt oceanic circulation changes: Trying to reconcile models and reconstructions, *Quat. Sci. Rev.*, *22*, 1647–1658.

Edwards, R., P. N. Sedwick, V. Morgan, C. F. Boutron, and S. Hong (1998), Iron in ice cores from Law Dome, East Antarctica: Implications for past deposition of aerosol iron, *Ann. Glaciol.*, *27*, 365–370.

EPICA Community Members (2004), Eight glacial cycles from an Antarctic ice core, *Nature*, *429*, 623–628.

EPICA Community Members (2006), One-to-one coupling of glacial climate variability in Greenland and Antarctica, *Nature*, doi:10.1038/nature05301, in press.

Fairbanks, R. G., R. A. Mortlock, T.-C. Chiu, L. Cao, A. Kaplan, T. P. Guilderson, T. W. Fairbanks, A. L. Bloom, P. M. Grootes, and M.-J. Nadeau (2005), Radiocarbon calibration curve spanning 0 to 50,000 years BP based on paired $^{230}Th/^{234}U/^{238}U$ and ^{14}C dates on pristine corals, *Quat. Sci. Rev.*, *24*, 1781–1796.

Farrell, J. W., and W. L. Prell (1989), Climate change and $CaCO_3$ preservation: An 800,000 year bathymetric reconstruction from the central equatorial Pacific Ocean, *Paleoceanography*, *4*, 447–466.

Field, C. V., G. A. Schmidt, D. Koch, and C. Salyk (2006), Modeling production and climate-related impacts on ^{10}Be concentration in ice cores, *J. Geophys. Res.*, *111*, D15107, doi:10.1029/2005JD006410.

Fischer, H., M. Wahlen, J. Smith, D. Mastroianni, and B. Deck (1999), Ice core records of atmospheric CO_2 around the last three glacial terminations, *Science*, *283*, 1712–1714.

Gaspari, V., C. Barbante, G. Cozzi, P. Cescon, C. F. Boutron, P. Gabrielli, G. Capodaglio, C. Ferrari, J. R. Petit, and B. Delmonte (2006), Atmospheric iron fluxes over the last deglaciation: Climatic implications, *Geophys. Res. Lett.*, *33*, L03704, doi:10.1029/2005GL024352.

Gersonde, R., X. Crosta, A. Abelmann, and L. Armand (2005), Sea-surface temperature and sea ice distribution of the Southern Ocean at the EPILOG Last Glacial Maximum — A circum-Antarctic view based on siliceous microfossil records, *Quat. Sci. Rev.*, *24*, 869–896.

Gnanadesikan, A., R. D. Slater, N. Gruber, and J. L. Sarmiento (2002), Oceanic vertical exchange and new production: A comparison between models and observations, *Deep Sea Res., Part II*, *49*, 363–401.

Goslar, T., M. Arnold, N. Tisnerat-Laborde, J. Czernik, and K. Wickowski (2000), Variations of Younger Dryas atmospheric radiocarbon explicable without ocean circulation changes, *Nature*, *403*, 877–880.

Hemming, S. R. (2004), Heinrich events: Massive late Pleistocene detritus layers of the North Atlantic and their global climate imprint, *Rev. Geophys.*, *42*, RG1005, doi:10.1029/2003RG000128.

Hodell, D. A., K. A. Venz, C. D. Charles, and U. S. Ninnemann (2003), Pleistocene vertical carbon isotope and carbonate gradients in the South Atlantic sector of the Southern Ocean, *Geochem. Geophys. Geosyst.*, *4*(1), 1004, doi:10.1029/2002GC000367.

Howard, W. R., and W. L. Prell (1994), Late Quaternary $CaCO_3$ production and preservation in the Southern Ocean:

Implications for oceanic and atmospheric carbon cycling, *Paleoceanography*, *9*, 453–482.

Hughen, K., S. Lehman, J. Southon, J. Overpeck, O. Marchal, C. Herring, and J. Turnbull (2004), ^{14}C activity and global carbon cycle changes over the past 50,000 years, *Science*, *303*, 202–207.

Hughen, K. A., J. R. Southon, S. J. Lehman, and J. T. Overpeck (2000), Synchronous radiocarbon and climate shifts during the last deglaciation, *Science*, *290*, 1951–1954.

Indermühle, A., et al. (1999), Holocene carbon-cycle dynamics based on CO_2 trapped in ice at Taylor dome, Antarctica, *Nature*, *398*, 121–126.

Indermühle, A., E. Monnin, B. Stauffer, and T. F. Stocker (2000), Atmospheric CO_2 concentration from 60 to 20 kyr BP from the Taylor Dome ice core, Antarctica, *Geophys. Res. Lett.*, *27*, 735–738.

Johnsen, S. J., H. B. Clausen, W. Dansgaard, K. Fuhrer, N. Gundestrup, C. U. Hammer, P. Iversen, J. Jouzel, B. Stauffer, and J. P. Steffensen (1992), Irregular glacial interstadials recorded in a new Greenland ice core, *Nature*, *359*, 311–313.

Joos, F., S. Gerber, I. C. Prentice, B. L. Otto-Bliesner, and P. J. Valdes (2004), Transient simulations of Holocene atmospheric carbon dioxide and terrestrial carbon since the Last Glacial Maximum, *Global Biogeochem. Cycles*, *18*, GB2002, doi:10.1029/2003GB002156.

Jouzel, J., F. Vimeux, N. Caillon, G. Delaygue, G. Hoffmann, V. Masson-Delmotte, and F. Parrenin (2003), Magnitude of isotope/temperature scaling for interpretation of central Antarctic ice cores, *J. Geophys. Res.*, *108*(D12), 4361, doi:10.1029/2002JD002677.

Kawamura, K., T. Nakazawa, S. Aoki, S. Sugawara, Y. Fujii, and O. Watanabe (2003), Atmopsheric CO_2 variations over the last three glacial-interglacial climatic cycles deduced from the Dome Fuji deep ice core, Antarctica using a wet extraction technique, *Tellus, Ser. B*, *55*, 126–137.

Kitagawa, H., and J. van der Pflicht (2000), Atmospheric radiocarbon calibration beyond 11,900 Cal BP from Lake Suigetsu laminated sediments, *Radiocarbon*, *42*, 369–380.

Knorr, G., and G. Lohmann (2003), Southern Ocean origin for the resumption of Atlantic thermohaline circulation during deglaciation, *Nature*, *424*, 532–536.

Knutti, R., J. Flückiger, T. F. Stocker, and A. Timmermann (2004), Strong hemispheric coupling of glacial climate through continental freshwater discharge and ocean circulation, *Nature*, *430*, 851–856.

Kohfeld, K. E., C. L. Quéré, S. Harrison, and R. F. Anderson (2005), Role of marine biology in glacial-interglacial CO_2 cycles, *Science*, *308*, 74–78.

Köhler, P., and H. Fischer (2004), Simulating changes in the terrestrial biosphere during the last glacial/interglacial transition, *Global Planet. Change*, *43*, 33–55, doi:10.1016/j.gloplacha.2004.02.005.

Köhler, P., and H. Fischer (2006a), Proposing a mechanistic understanding of changes in atmospheric CO_2 during the last 740,000 years, *Clim. Past Discuss.*, *2*, 1–42. (Available at http://direct.sref.org/1814-9359/cpd/2006-2-1)

Köhler, P., and H. Fischer (2006b), Simulating low frequency changes in atmospheric CO_2 during the last 740 000 years, *Clim. Past*, *2*, 57–78. (Available at http://direct.sref.org/1814-9332/cp/2006-2-57)

Köhler, P., H. Fischer, G. Munhoven, and R. E. Zeebe (2005a), Quantitative interpretation of atmospheric carbon records over the last glacial termination, *Global Biogeochem. Cycles*, *19*, GB4020, doi:10.1029/2004GB002345.

Köhler, P., F. Joos, S. Gerber, and R. Knutti (2005b), Simulated changes in vegetation distribution, land carbon storage, and atmospheric CO_2 in response to a collapse of the North Atlantic thermohaline circulation, *Clim. Dyn.*, *25*, 689–708, doi:10.1007/s00382-005-0058-8.

Köhler, P., J. Schmitt, and H. Fischer (2006), On the application and interpretation of Keeling plots in paleo climatic research — Deciphering $\delta^{13}C$ of atmospheric CO_2 measured in ice cores, *Biogeosci. Discuss.*, *3*, 513–573. (Available at http://direct.sref.org/1810-6285/bgd/2006-3-513)

Kok, Y. S. (1999), Climatic influence in NRM and ^{10}Be-derived geomagnetic paleointensity data, *Earth Planet. Sci. Lett.*, *166*, 105–119.

Kutzbach, J., R. Gallimore, S. Harrison, P. Behling, R. Selin, and F. Laarif (1998), Climate and biome simulations for the past 21,000 years, *Quat. Sci. Rev.*, *17*, 473–506.

Labeyrie, L. D., J. C. Duplessy, and P. L. Blanc (1987), Variations in mode of formation and temperature of oceanic deep waters over the past 125,000 years, *Nature*, *327*, 477–482.

Laj, C., C. Kissel, A. Mazaud, J. E. T. Channell, and J. Beer (2000), North Atlantic palaeointensity stack since 75 ka (NAPIS-75) and the duration of the Laschamp event, *Philos. Trans. Soc London, R., Ser. A*, *358*, 1009–1025.

Laj, C., C. Kissel, A. Mazaud, E. Michel, R. Muscheler, and J. Beer (2002), Geomagnetic field intensity, North Atlantic Deep Water circulation and atmospheric $\Delta^{14}C$ during the last 50 kyr, *Earth Planet. Sci. Lett.*, *200*, 177–190.

Laj, C., C. Kissel, and J. Beer (2005), High resolution global paleointensity stack since 75 kyr (GLOPIS-75) calibrated to absolute values, in *Timescales of the Paleomagnetic Field*, *Geophys. Monogr. Ser.*, vol. 145, edited by J. E. T. Channell et al., pp. 255–265, AGU, Washington, D. C.

Lal, D., and B. Peters (1967), Cosmic ray produced radioactivity on the Earth, in *Handbuch für Physik*, vol. 46/2, edited by S. Flügge, pp. 551–612, Springer, New York.

Lambeck, K., and J. Chappell (2001), Sea level change through the last glacial cycle, *Science*, *292*, 679–686.

Lisiecki, L. E., and M. E. Raymo (2005), A Pliocene-Pleistocene stack of 57 globally distributed benthic $\delta^{18}O$ records, *Paleoceanography*, *20*, PA1003, doi:10.1029/2004PA001071.

Marchal, O., T. F. Stocker, and R. Muscheler (2001), Atmospheric radiocarbon during the Yonger Dryas: Production, ventilation, or both?, *Earth Planet. Sci. Lett.*, *185*, 383–395.

Marchitto, T. M., J. Lynch-Stieglitz, and S. R. Hemming (2005), Deep Pacific $CaCO_3$ compensation and glacial-interglacial atmospheric CO_2, *Earth Planet. Sci. Lett.*, *231*, 317–336.

Martin, J. H. (1990), Glacial-interglacial CO_2 change: The iron hypothesis, *Paleoceanography*, *5*, 1–13.

Masarik, J., and J. Beer (1999), Simulation of particle fluxes of cosmogenic nuclide production in the Earth's atmosphere, *J. Geophys. Res*, *104*(D10), 12,099–12,111.

Matsumoto, K., J. L. Sarmiento, and M. A. Brzezinski (2002), Silicic acid leakage from the Southern Ocean: A possible explanation for glacial atmospheric pCO_2, *Global Biogeochem. Cycles*, *16*(3), 1031, doi:10.1029/2001GB001442.

McManus, J. F., R. Francois, J.-M. Gheradi, L. D. Keigwin, and S. Brown-Leger (2004), Collapse and rapid resumption of Atlantic meridional circulation linked to deglacial climate changes, *Nature*, *428*, 834–837.

Meissner, K. J., A. Schmittner, A. J. Weaver, and J. F. Adkins (2003), Ventilation of the North Atlantic Ocean during the Last Glacial Maximum: A comparison between simulated and observed radiocarbon ages, *Paleoceanography*, *18*(2), 1023, doi:10.1029/2002PA000762.

Monnin, E., A. Indermühle, A. Dällenbach, J. Flückiger, B. Stauffer, T. F. Stocker, D. Raynaud, and J.-M. Barnola (2001), Atmospheric CO_2 concentrations over the last glacial termination, *Science*, *291*, 112–114.

Monnin, E., et al. (2004), Evidence for sustantial accumulation rate variability in Antarctica during the Holocene, through synchronization of CO_2 in the Taylor Dome, Dome C and DML ice cores, *Earth Planet. Sci. Lett.*, *224*, 45–54.

Munhoven, G. (2002), Glacial-interglacial changes of continental weathering: Estimates of the related CO_2 and HCO_3^- flux variations and their uncertainties, *Global Planet. Change*, *33*, 155–176.

Muscheler, R., J. Beer, G. Wagner, and R. C. Finkel (2000), Changes in deep-water formation during the Younger Dryas event inferred from ^{10}Be and ^{14}C records, *Nature*, *408*, 567–570.

Muscheler, R., J. Beer, G. Wagner, C. Laj, C. Kissel, G. M. Raisbeck, F. Yiou, and P. W. Kubik (2004), Changes in the carbon cycle during the last deglaciation as indicated by the comparison of ^{10}Be and ^{14}C records, *Earth Planet. Sci. Lett.*, *219*, 325–340.

Muscheler, R., J. Beer, P. W. Kubik, and H.-A. Synal (2005), Geomagnetic field intensity during the last 60,000 years based on ^{10}Be and ^{36}Cl from the Summit ice cores and ^{14}C, *Quat. Sci. Rev.*, *24*, 1849–1860, doi:10.1016/j.quascirev.2005.01.012.

NorthGRIP Members (2004), High-resolution record of Northern Hemisphere climate extending into the last interglacial period, *Nature*, *431*, 147–151.

Petit, J. R., et al. (1999), Climate and atmospheric history of the past 420,000 years from the Vostok ice core, Antarctica, *Nature*, *399*, 429–436.

Pflaumann, U., et al. (2003), Glacial North Atlantic: Sea-surface conditions reconstructed by GLAMAP 2000, *Paleoceanography*, *18*(3), 1065, doi:10.1029/2002PA000774.

Rahmstorf, S. (2002), Ocean circulation and climate during the paste 120,000 years, *Nature*, *419*, 207–214.

Reimer, P. J., et al. (2004), INTCAL04 terrestrial radiocarbon age calibration, 0–26 Cal kyr BP, *Radiocarbon*, *46*, 1029–1058.

Ridgwell, A. J. (2003), Implications of the glacial CO_2 "iron hypothesis" for Quaternary climate change, *Geochem. Geophys. Geosyst.*, *4*(9), 1076, doi:10.1029/2003GC000563.

Ridgwell, A. J., A. J. Watson, M. A. Maslin, and J. O. Kaplan (2003), Implications of coral reef buildup for the controls on atmospheric CO_2 since the Last Glacial Maximum, *Paleoceanography*, *18*(4), 1083, doi:10.1029/2003PA000893.

Robinson, L. R., J. F. Adkins, L. D. Keigwin, J. Southon, D. P. Fernandez, S.-L. Wang, and D. S. Scheirer (2005), Radiocarbon variability in the western North Atlantic during the last deglaciation, *Science*, *310*, 1469–1473, doi:10.1126/science.1114832.

Ruddiman, W. F. (2003), The anthropogenic greenhouse era began thousands of years ago, *Clim. Change*, *61*, 261–293.

Sarnthein, M., U. Pflaumann, and M. Weinelt (2003), Past extent of sea ice in the northern North Atlantic inferred from foraminiferal paleotemperature estimates, *Paleoceanography*, *18*(2), 1047, doi:10.1029/2002PA000771.

Schmittner, A. (2005), Decline of the marine ecosystem caused by a reduction in the Atlantic overturning circulation, *Nature*, *434*, 628–633.

Schramm, A., M. Stein, and S. L. Goldstein (2000), Calibration of the ^{14}C time scale to 440 ka by ^{234}U-^{230}Th dating of Lake Lisan sediments (last glacial Dead Sea), *Earth Planet. Sci. Lett.*, *175*, 27–40.

Shackleton, N. (2000), The 100,000-year ice-age cycle identified and found to lag temperature, carbon dioxide, and orbital eccentricity, *Science*, *289*, 1897–1902.

Shackleton, N. J., A. Berger, and W. P. Peltier (1990), An alternative astronomical calibration of the lower Pleistocene timescale based on OPD site 677, *Trans. R. Soc. Edinburgh Earth Sci.*, *81*, 251–261.

Siegenthaler, U., M. Heimann, and H. Oeschger (1980), ^{14}C variations caused by changes in the global carbon cycle, *Radiocarbon*, *22*, 177–191.

Siegenthaler, U., et al. (2005), Stable carbon cycle-climate relationship during the late Pleistocene, *Science*, *310*, 1313–1317, doi:10.1126/science.1120130.

Sigman, D. M., and E. A. Boyle (2000), Glacial/interglacial variations in atmospheric carbon dioxide, *Nature*, *407*, 859–869.

Smith, H. J., H. Fischer, M. Wahlen, D. Mastroianni, and B. Deck (1999), Dual modes of the carbon cycle since the Last Glacial Maximum, *Nature*, *400*, 248–250.

Stocker, T. F., and S. J. Johnsen (2003), A minimum thermodynamic model for the bipolar seesaw, *Paleoceanography*, *18*(4), 1087, doi:10.1029/2003PA000920.

Stuiver, M., P. J. Reimer, E. Bard, J. W. Beck, G. S. Burr, K. A. Hughen, B. Kromer, G. McCormac, J. van der Plicht, and M. Spurk (1998), INTCAL98 radiocarbon age calibration, 24,000-0 cal BP, *Radiocarbon*, *40*, 1041–1083.

Vecsei, A., and W. H. Berger (2004), Increase of atmospheric CO_2 during deglaciation: Constraints on the coral reef hypothesis from patterns of deposition, *Global Biogeochem. Cycles*, *18*, GB1035, doi:10.1029/2003GB002147.

Visser, K., R. Thunell, and L. Stott (2003), Magnitude and timing of temperature change in the Indo-Pacific warm pool during deglaciation, *Nature*, *421*, 152–155.

Voelker, A. H. L., M. Sarnthein, P. Grootes, H. Erlenkeuser, C. Laj, A. Mazaud, M.-J. Nadeau, and M. Schleicher (1998), Correlation of marine ^{14}C ages from the nordic seas with the GISP2 isotope record: Implications for radiocarbon calibration beyond 25 kyr BP, *Radiocarbon*, *40*, 517–534.

Wagner, G., J. Beer, C. Laj, C. Kissel, J. M. an R. Muscheler, and H.-A. Synal (2000), Chlorine-36 evidence for the Mono Lake event in the summit GRIP ice core, *Earth Planet. Sci. Lett.*, *181*, 1–6.

Wagner, G., C. Laj, J. Beer, C. Kissel, R. Muscheler, J. Masarik, and H.-A. Synal (2001), Reconstruction of the paleoaccumulation rate of central Greenland during the last 75 kyr using the cosmogenic radionuclides ^{36}Cl and ^{10}Be and geomagnetic field intensity data, *Earth Planet. Sci. Lett.*, *193*, 515–521.

Watson, A. J., and A. C. Naveira-Garabato (2006), The role of Southern Ocean mixing and upwelling in glacial-interglacial atmospheric CO_2 change, *Tellus, Ser. B*, *58*, 73–87.

Wolff, E. W., J. A. Chappellaz, H. Fischer, C. Krull, H. Miller, T. Stocker, and A. J. Watson (2004), The EPICA challenge to the Earth system modeling community, *Eos Trans. AGU*, *85*(38), 363.

Wolff, E. W., et al. (2005), Modeling past atmospheric CO_2: Results of a challenge, *Eos Trans. AGU*, *86*(38), 341, 345.

Wolff, E. W., et al. (2006), Southern Ocean sea-ice extent, productivity and iron fluxes over the past eight glacial cycles, *Nature*, *440*, 491–496, doi:10.1038/nature04614.

Yang, S., H. Odah, and J. Shaw (2000), Variations in the geomagnetic dipole moment over the last 12000 years, *Geophys. J. Int.*, *140*, 158–162.

Yiou, F., et al. (1997), Beryllium-10 in the Greenland Ice Core Project ice core at Summit, Greenland, *J. Geophys. Res.*, *102*, 26,783–26,794.

Zeebe, R. E., and D. A. Wolf-Gladrow (2001), *CO_2 in Seawater: Equilibrium, Kinetics, Isotopes*, *Elsevier Oceanogr. Book Ser.*, vol. 65, 346 pp., Elsevier, New York.